

AD A125335

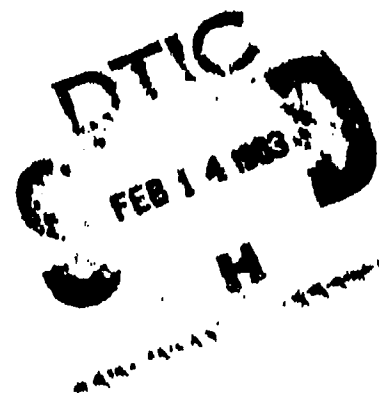
125335
12
AD

TECHNICAL REPORT ARBRL-TR-02466

A MODEL OF ANTIFRATRICIDE SHIELD
INTERACTION WITH JETS FORMED BY MULTIPLE
ARTILLERY ROUND DETONATIONS

Evan Harris Walker

January 1983



US ARMY ARMAMENT RESEARCH AND DEVELOPMENT COMMAND
BALLISTIC RESEARCH LABORATORY
ABERDEEN PROVING GROUND, MARYLAND

Approved for public release; distribution unlimited.

DTIC FILE COPY

83 03 11 037

Destroy this report when it is no longer needed.
Do not return it to the originator.

Secondary distribution of this report is prohibited.

Additional copies of this report may be obtained
from the National Technical Information Service,
U. S. Department of Commerce, Springfield, Virginia
22161.

The findings in this report are not to be construed as
an official Department of the Army position, unless
so designated by other authorized documents.

*The use of trade names or manufacturers' names in this report
does not constitute endorsement of any commercial product.*

REPORT DOCUMENTATION PAGE		READ INSTRUCTIONS BEFORE COMPLETING FORM
1. REPORT NUMBER TECHNICAL REPORT ARBRL-TR-02466	2. GOVT ACCESSION NO. AD-A125 335	3. RECIPIENT'S CATALOG NUMBER
4. TITLE (and Subtitle) A MODEL OF ANTIFRATRICIDE SHIELD INTERACTION WITH JETS FORMED BY MULTIPLE ARTILLERY ROUND DETONATIONS		5. TYPE OF REPORT & PERIOD COVERED Final
7. AUTHOR(s) Evan Harris Walker		6. PERFORMING ORG. REPORT NUMBER
9. PERFORMING ORGANIZATION NAME AND ADDRESS US Army Ballistic Research Laboratory ATTN: DRDAR-BLT Aberdeen Proving Ground, MD 21005		10. PROGRAM ELEMENT, PROJECT, TASK AREA & WORK UNIT NUMBERS 1L162618AH80
11. CONTROLLING OFFICE NAME AND ADDRESS US Army Armament Research and Development Command US Army Ballistic Research Laboratory (DRDAR-BL) Aberdeen Proving Ground, MD 21005		12. REPORT DATE January 1983
		13. NUMBER OF PAGES 53
14. MONITORING AGENCY NAME & ADDRESS (if different from Controlling Office)		15. SECURITY CLASS. (of this report) UNCLASSIFIED
16. DISTRIBUTION STATEMENT (of this Report) Approved for public release, distribution unlimited.		15a. DECLASSIFICATION/DOWNGRADING SCHEDULE
17. DISTRIBUTION STATEMENT (of the abstract entered in Block 20, if different from Report)		
18. SUPPLEMENTARY NOTES		
19. KEY WORDS (Continue on reverse side if necessary and identify by block number) Isolation Panels Munitions Transport Sympathetic Detonation Mass Detonation Buffer Materials Round to Round Propagation Munition Storage Buffer Design Artillery Shell Storage Munition Shielding Shield Design Fratricide Shield Design Fragmentation Hazards Shield Materials Metal Jets		
20. ABSTRACT (Continue on reverse side if necessary and identify by block number) (kjm) This report presents a theoretical model of certain influence attenuation effects involved in round to round detonation propagation. The purpose of the model is to provide guidance in the design of structures to safely store and transport HE filled munitions. Such structures employing isolation panels or shields between artillery shells or groups of artillery shells are to prevent the propagation of detonations in the event that one or several shells are detonated by other means. The most severe effect to be shielded against is the		

UNCLASSIFIED

SECURITY CLASSIFICATION OF THIS PAGE(When Data Entered)

metal jetting produced when neighboring shells are simultaneously detonated. The present report deals with the interaction that occurs between such metal jets and multi-layered shields composed of inert materials, explosive layers, or semiactive (hydrated) materials that derive their energy from the kinetic energy of the impacting metal jet and shell casing fragments. The study finds that the model correctly reproduces most features found in experiments with isolation panels, that present semiactive materials such as gypsum show only minor enhancement of shield performance, and that the use of proper positioning of panels and distribution of shield material is a significant parameter for the design of such structures.

UNCLASSIFIED

SECURITY CLASSIFICATION OF THIS PAGE(When Data Entered)

TABLE OF CONTENTS

	Page
LIST OF ILLUSTRATIONS	5
I. INTRODUCTION	7
II. DESCRIPTION OF THE ARTILLERY SHELL METAL JET	8
III. ARTILLERY SHELL INFLUENCE INITIATION EFFECTS	8
IV. DESCRIPTION OF THE INFLUENCE SUPPRESSIVE STRUCTURE PARAMETERS FOR THE ARTILLERY SHELL PACKAGING AND STORAGE SHIELDS	10
V. SHOCK ACTIVATION AND JET PENETRATION OF HYDRATED OR EXPLOSIVE SOLIDS	12
VI. DESIGN OPTIMIZATION FORMULATION FOR INFLUENCE ATTENUATION PANELS TO SUPPRESS SHELL - SHELL IMPACT JET INDUCED INITIATION	18
VII. COMPUTATIONS	25
VIII. COMPARISON WITH EXPERIMENTAL RESULTS	30
IX. CONCLUSIONS	38
APPENDIX - PROGRAM "MAIN"	41
DISTRIBUTION LIST	51

Accession For	
NTIS GRA&I	<input checked="checked" type="checkbox"/>
DTIC TAB	<input type="checkbox"/>
Unannounced	<input type="checkbox"/>
Justification	
By	
Distribution/	
Availability Codes	
Dist	Avail and/of Special
A	



LIST OF ILLUSTRATIONS

Figure	Page
1. Flash X-ray Photograph of two Comp B Filled Steel Pipe Bombs From End-on View	9
2. General Configuration of Shields Treated in the Present Paper	11
3. Schematic of an Inelastic Collision Between an Inert Plate Impacting a Plate Containing Water Content	13
4. Schematic of a Jet Interaction With a Target Material Under Conditions of Hypervelocity Flow	15
5. Schematic of the Jet Formed by Simultaneously Initiated Artillery Shells and Antifratricide Panels Defining the Important Parameters Governing the Interaction	19
6. Nondimensional Penetration P'/R Versus Nondimensional Shield Thickness C/R , Where Shield is Placed at Midpoint Between Donor and Acceptor Rounds Separated by 1.0 R	26
7. Nondimensional Penetration P'/R Versus Nondimensional Shield Thickness C/R , Where Shield is Placed at Midpoint Between Donor and Acceptor Rounds Separated by 2.0 R	27
8. Nondimensional Penetration P'/R Versus Nondimensional Shield Thickness C/R , Where Shield is Placed at Midpoint Between Donor and Acceptor Rounds Separated by 3.0 R	28
9. Nondimensional Penetration P'/R Versus Nondimensional Shield Thickness C/R , Where Shield is Placed at Midpoint Between Donor and Acceptor Rounds Separated by 4.0 R	29
10. Nondimensional Penetration P'/R Versus Nondimensional Panel Separation Distance D/R for two Symmetrically Placed 0.53 R Thick Panels in a 4.0 R Space Between Donors and Target Plate for Various Panel Densities	31
11. Nondimensional Penetration P'/R Versus Nondimensional Total Shield Thickness $(C + C')R$, Where the Shield Consists of Two Panels Symmetrically Placed About the Midpoint, one Against the Donor Rounds, one Against the Acceptor Rounds (or Witness Plate). Donor-Acceptor Separation is 1.0 R	32
12. Nondimensional Penetration P'/R Versus Nondimensional Total Shield Thickness $(C + C')R$, Where the Shield Consists of Two Panels Symmetrically Placed About the Midpoint, one Against the Donor Rounds, one Against the Acceptor Rounds (or Witness Plate). Donor-Acceptor Separation is 2.0 R	33

LIST OF ILLUSTRATIONS (continued)

Figure	Page
13. Nondimensional Penetration P'/R Versus Nondimensional Total Shield Thickness $(C + C')R$, Where the Shield Consists of Two Panels Symmetrically Placed About the Midpoint, one Against the Donor Rounds, one Against the Acceptor Rounds (or Witness Plate). Donor-Acceptor Separation is 3.0 R	34
14. Nondimensional Penetration P'/R Versus Nondimensional Total Shield Thickness $(C + C')R$, Where the Shield Consists of Two Panels Symmetrically Placed About the Midpoint, one Against the Donor Rounds, one Against the Acceptor Rounds (or Witness Plate). Donor-Acceptor Separation is 4.0 R	35
15. Nondimensional Penetration Versus Density for a "Foam" Filling The Space Between the Donor Rounds and Target Plate (Acceptor Rounds) for a gap of 4.0 R	36
16. Penetration Depth in mm Charted for the Several Experimental Shield Tests	37

I. INTRODUCTION

This report deals with the problem of optimizing the packaging for artillery shells to provide protection against influence initiation in the metal jetting environment produced by shell casing impacts. The initiation of a shell stored or transported with other shells produces high speed casing fragments that on impact with nearby shells can cause shocks, penetration, and/or fracture resulting in the initiation of the explosive fill in the neighboring shells. In addition, the detonation of two adjoining shells can, as their casings impact, produce significant metal jetting. In the case of 155 mm artillery shells this metal jet can cut through as much as 15 cm of steel. As such, this latter mechanism represents the most severe fratricide environment constraining shield design. Neighboring shells can be protected from this jet of material by inserting layers of material to intercept and disrupt the metal jet. The insertion of material, however, greatly increases the total amount of material required for the safe packaging of munitions. It becomes important, therefore, to develop a model of the shield interaction with such shell casing jets to facilitate the development of optimum packaging designs capable of inhibiting influence initiation of shells in this severe environment.

The design of an optimum packaging involves variation of numerous parameters such as number, thickness, composition, and placement of the shield materials. Extensive experimental work has been carried out to determine good potential designs¹⁻⁴. Still, determination of an optimum design requires the development of a mathematical model to minimize the total number of experimental tests necessary for the development of the influence suppression configuration. The purpose of the present report is to provide a model of the antifratricide shield panels subjected to the most severe environment, jets produced by simultaneously detonating neighboring rounds. A subsequent report will deal with the problem of shock attenuation by panels separating neighboring rounds.

¹Howe, P.M., "The Phenomenology of Interround Communication and Techniques For Prevention," ARBRL-TR-02048 (1978) (AD#A054373).

²Howe, P.M., Collis, D., "Effectiveness of Plastic Shields in Prevention of Propagation of Reaction Between Compartmentalised Warheads," ARBRL-MR-02827 (1978) (AD#B027466L).

³Howe, P.M., "The Response of Munitions to Impact," ARBRL-TR-02169 (1979) (AD#B040230).

⁴Gibbons, Jr., Gould, "Multiple Round Fragmentation Hazards and Shielding," ARBRL-TR-02329 (1981). (AD #B058793L)

II. DESCRIPTION OF THE ARTILLERY SHELL METAL JET

The mechanism causing influence initiation of concern in the present report is the jetting of metal due to the impact of shell casing material from two neighboring shells initiated at approximately the same time. An example of the formation of a jet resulting from the simultaneous detonation of two Comp B filled steel pipe bombs (15.2 cm long, 4.83 cm diameter, 3.2 mm thick wall) is seen in the end-on flash X-ray photograph, Fig. 1. The details of the jets formed by this mechanism vary considerably from shot to shot (largely because the pipe bombs are not precision items). Typically, the jets travel at about 2 km/s with the lowest velocity material effective in penetrating metal plates traveling at about 0.5 km/s. Material in the jet is confined to a fan of material about 0.1 radian in angular width.

The design of an optimum suppressive structure requires that this type of jet be either interrupted, dissipated or inhibited. We describe below the model used to calculate the effect of jet collision with elements of the suppressive structure.

III. ARTILLERY SHELL INFLUENCE INITIATION EFFECTS

Impact of explosively accelerated metal on artillery shells can produce influence initiation by any of the following mechanisms:

(1) Shock loading of the explosive arising from metal on metal impact leading to the incidence of a strong shock propagating into the explosive.

(2) Adiabatic compression or plastic flow heating of the explosive (or entrapped gas) due to compressive deformation of the impacted shell or to fragment penetration.

(3) Plastic flow heating of explosive injected into shell fissures formed by metal on metal impact.

(4) Direct exposure of the explosive fill to hot fragments in the explosive environment due to shell wall failure or penetration.

These mechanisms entail different quantitative criteria to determine if initiation will be produced in a given test situation. These include:

(1) The time integral of the shock pressure p squared, $\int p^2 dt$. This quantity can be compared with critical values for different explosives.

(2) The maximum pressure to which the explosive is subjected during shock loading, p_{\max} , and the rate of loading dp/dt of the explosive or entrapped gas.

(3) A shell deformation characteristic measure Δ ,

$$\Delta = \iint \frac{p - \sigma}{\rho} dt dt$$

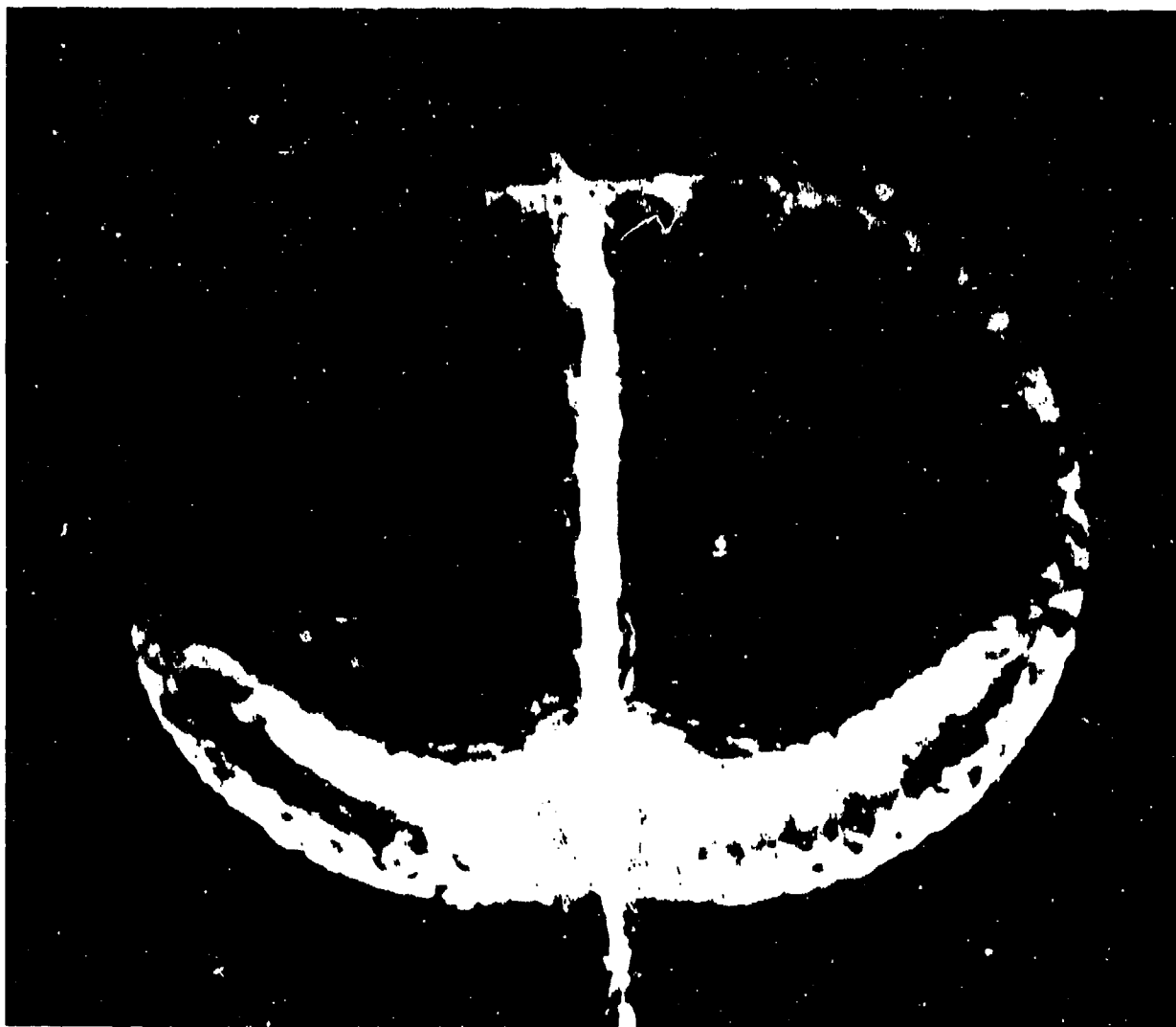


Figure 1. Flash X-ray photograph of two Comp B filled steel pipe bombs from end-on view. The pipe bombs are 15.2 cm long, 4.83 cm in diameter with 3.2 mm thick walls and separated by a distance of 6.35 mm. The flash X-ray was taken 50.1 μ s after detonation of the rounds. The vertical stripe in the X-ray photograph is caused by the metal jet, which of course, is traveling with a velocity gradient.

where σ is the effective strength of the shell wall material (taking account of moment arm effects in the loading), and ρ is the density of the material.

(4) Depth of penetration of impacting fragments or jets into the casing of the artillery shell.

In the present report we will only be concerned with the last of these, the penetration depth into the wall, as from the experimental data it appears that this is the most critical measure in determining whether or not metal jetting will lead to HE initiation.

IV. DESCRIPTION OF THE INFLUENCE SUPPRESSIVE STRUCTURE PARAMETERS FOR THE ARTILLERY SHELL PACKAGING AND STORAGE SHIELDS

Experimental tests^{3,4} have demonstrated that the use of multiple sheets of material (perpendicular to the line joining the center of the detonated or donor shell and the protected or acceptor shell) proves to be effective in suppressing influence initiation. Plaster, containing water of hydration, has appeared to be a particularly good material for use in these experiments.⁴ In addition the use of explosive material sandwiched between layers of inert material may prove to be a good material to shield artillery shells from metal jets. As such, a typical shield design may have as many as six layers, each of which must be designed to be of optimum thickness and placement. Figure 2 shows the general configuration to be treated in the present paper. Since plaster contains water of hydration, there is the possibility for it to behave as an active material in these structures. The high velocity impact of metal from an exploding shell gives rise to shocks in the plaster, producing shock heating of the material. This heating can liberate water from the gypsum in the form of steam, driving the material as though it had exploded.

In the following treatment of the suppressive structure, Fig. 2 will be used as the basis for the physical configuration to be treated by the model. For the most part, materials, dimensions, etc. will be represented parametrically. Subsequently the model will be exercised to determine those characteristics yielding the best results under various constraints (such as total weight or volume).

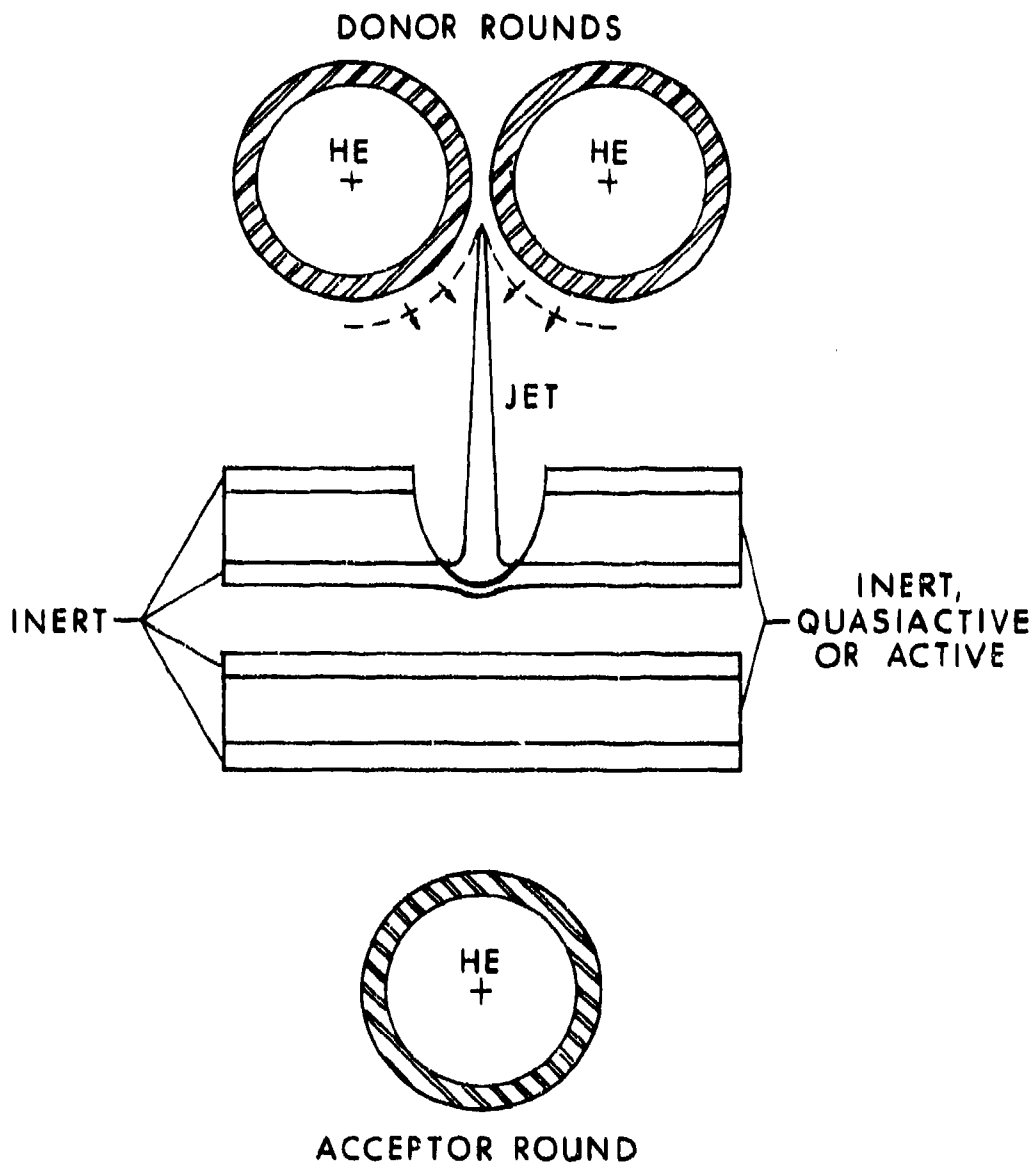


Figure 2. General configuration of shields treated in the present paper. The donor shells are assumed placed in the worst case position relative to the acceptor shell. Two shields each of up to three layers of any thickness are assumed placed at any position between the donor and acceptor shells. The middle layer of each shield is assumed to consist of an inert material, a semiactive material such as plaster with water of hydration, or an explosive material.

V. SHOCK ACTIVATION AND JET PENETRATION OF HYDRATED OR EXPLOSIVE SOLIDS

Use of gypsum in the form of plaster panels has yielded some experimental data⁴, suggesting that under shock loading the material responds in an explosive manner. Sufficiently strong shock can give rise to the heating of the granular solid material comprising these panels. The heat acts to calcine the plaster giving rise to a high temperature steam under elevated pressures. As a result some of the original shock energy can be dissipated in the plaster. The subsequent explosive expansion of the plaster, however, may give rise to shocks in neighboring materials. Shocks propagating through water, however, have not exhibited any increased ability to attenuate shocks from donor rounds. Thus, there may exist an effect due to shock induced calcination that involves the "solid residuum" serving as the source of the heat available for the generation of the steam.

Let us assume that we have a completely inelastic collision between a plate of areal density σ_1 (volumetric density ρ_1) traveling at an initial velocity v_1 and a stationary plaster plate of areal density σ_2 (volumetric density ρ_2) containing a fraction g of moisture as shown in Fig. 3. After the collision the velocity (of the center of mass) is v_2 . The energy absorbed per unit area E is given by

$$E = \frac{1}{2} [P_1^2/\sigma_1 - P_2^2/(\sigma_1 + \sigma_2)] \quad (1)$$

where

$$P_1 = \sigma_1 v_1 \quad (2)$$

and

$$P_2 = (\sigma_1 + \sigma_2) v_2 \quad (3)$$

The specific energy ϵ_2 , per unit mass in the second (plaster) plate before expansion is

$$\epsilon_2 = E/\sigma_2 \quad (4)$$

This energy gives rise to the heating of the "solid residuum" of specific heat C_{v_s} (which for plaster has a value of 0.210 cal/g°C), and the water of specific heat $C_{v_{H_2O}}$ (≈ 0.48 cal/g°K) that is liberated as the gypsum is heated. The heat of liberation is represented by h_f . For gypsum, h_f is 58.1 cal/g; for water, 79.7 cal/g. We obtain

$$\epsilon_2 = (1 - g)C_{v_s} \Delta T + C_{v_{H_2O}} \Delta T + gh_f \quad (5)$$

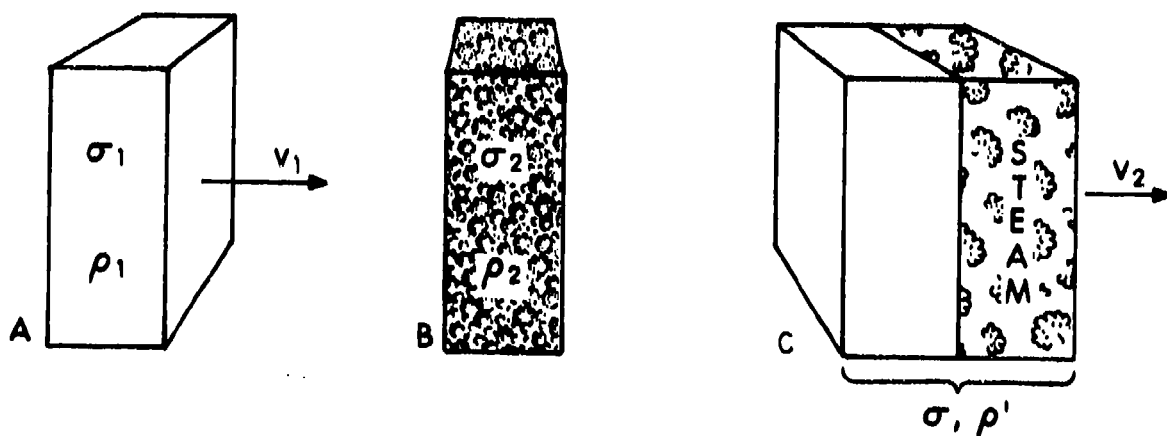


Figure 3. Schematic of an inelastic collision between an inert plate, A, traveling with velocity v_1 impacting on a plate containing water (for example, a plaster panel containing water of hydration) content, B. The resultant combination of plates, C, travels away with a velocity v_2 , the kinetic energy absorbed by the inelastic collision being converted to heat with the evolution of steam.

(This expression represents the unexpanded condition of the heated plaster so that the heat of vaporization does not occur here.) where $\Delta T = T - T_i$, T_i being the initial temperature of the plaster and T the temperature to which an amount ϵ_2 of energy heats the plaster. Of this, an energy (specific) ϵ_{H_2O} will be available as the explosively released energy of the steam. Where $gC_{v_{H_2O}} \Delta T$ is the energy that goes into heating the liberated water, the available energy is

$$\epsilon_{H_2O} = gC_{v_{H_2O}} \Delta T n \quad (6)$$

where n is the work efficiency. We will use for n the ideal thermodynamic efficiency (for a Carnot cycle) although the actual efficiency is lower. The ideal efficiency is

$$n = \frac{T - T_i}{T} \quad (7)$$

Where T is high, Eq. (8) serves as a good approximation. Thus, we can write

$$2\epsilon_{H_2O}/n = [\sigma_1 v_1^2 - (\sigma_1 + \sigma_2)v_2^2]/\sigma_2 - 2[(1 - g)C_{v_s} \Delta T + gh_f] \quad (8)$$

or substituting for ΔT from Eq. (8) and solving for ϵ_{H_2O} we have

$$2\epsilon_{H_2O} = n \left\{ \sigma_2 [\sigma_1 v_1^2 - (\sigma_1 + \sigma_2)v_2^2] - 2gh_f \right\} / \left[1 + \left(\frac{1 - g}{g} \right) \frac{C_{v_s}}{C_{v_{H_2O}}} \right] \quad (9)$$

The quantity $2\epsilon_{H_2O}$ can be used as the energy constant in the Gurney equation

in order to calculate the subsequent expansion of the plaster plate as it drives adjoining plates. It should be noted that the assumption of complete inelastic collision leads to Eq. (5) giving the energy available for calcination of the gypsum. In the case where a given shock propagates into a panel, it is necessary to determine the rate at which shock energy is converted to heat which will be a function of $(1 - g)$. The value for dry gypsum (water of hydration) is 0.209. Measurements by Gould Gibbons, Jr. (TBD - EEB) yielded a value of 0.290 for wet plaster as tested.

Let us now consider what occurs when a high velocity jet of material impacts a material such as plaster which explosively releases energy. Figure 4 shows the flow of jet material and target material in the coordinate system moving with the stagnation point in a target under steady state flow conditions. Letting v_j be the velocity of the jet and V_s the velocity of the stagnation point, in the frame of reference moving with the stagnation point, the jet approaches the stagnation point S with a velocity $v_j - V_s$ while the target material approaches with a velocity V_s . To maintain steady state

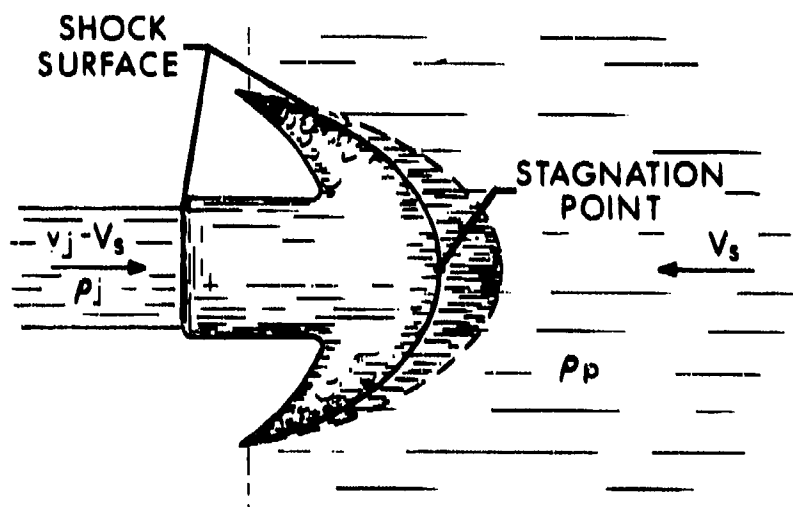


Figure 4. Schematic of a jet interaction with a target material under conditions of hypervelocity flow. Velocity vectors give velocities with respect to a coordinate system moving to the right with the stagnation velocity V_s .

flow, the forces acting on the stagnation point must be balanced. Therefore, we can write, noting that the shocked plaster gives rise to a pressure p_{H_2O} ,

$$\frac{1}{2}\rho_j(v_j - V_s)^2 = \frac{1}{2}\rho_1 V_s^2 + p_{H_2O} \quad (10)$$

We note that p_{H_2O} is simply equal to the energy density of the steam, ϵ_{H_2O} , as given by Eq. (9). By reference to Fig. 3 and recognizing that in jet penetration to an incremental depth dP an incremental length of penetrator dL impacts with the target and is consumed, we see that the quantities σ_1 and σ_2 of Eq. (9) take the values

$$\sigma_1 \rightarrow dL\rho_j \quad (11)$$

and

$$\sigma_2 \rightarrow dP\rho_p \quad (12)$$

Where

$$v_1 = v_j \quad (13)$$

we have

$$\sigma_1 v_1 = (\sigma_1 + \sigma_2) v_2 \quad (14)$$

or

$$v_2 = v_j / (1 + \frac{\sigma_2}{\sigma_1}) = v_j (1 + \frac{dP\rho_p}{dL\rho_j}) \quad (15)$$

Therefore, we have the integral expression for P

$$P = \int_0^L dL \sqrt{\rho / (1 + \alpha)} \quad (16)$$

where

$$\rho = \rho_j / \rho_p \quad (17)$$

$$\alpha = 2p_{H_2O} / \rho_p V_s^2 \quad (18)$$

and

$$p_{H_2O} = \rho_p \epsilon_{H_2O} \quad (19)$$

Where ρ and α are constant, we can write (16) as

$$P = L \sqrt{\rho/(1 + \alpha)}. \quad (20)$$

Substituting from (13) and (14) into (9) gives

$$\epsilon_{H_2O} = \frac{1}{2}nk \left[v_j^2 \left(\frac{\sigma_1}{\sigma_2} - \frac{\sigma_2}{\sigma_1 + \sigma_2} \right) - 2gh_f \right] \quad (21)$$

where

$$k = \left[1 + \frac{(1 - g)C_{vs}}{gC_{v_{H_2O}}} \right]^{-1}. \quad (22)$$

Defining

$$f = \sigma_1/\sigma_2 = \rho \frac{dL}{dP}, \quad (23)$$

we can write (21) as

$$\epsilon_{H_2O} = \frac{1}{2}nk \left[v_j^2 \left(\frac{f^2 + f - 1}{1 + f} \right) - 2gh_f \right]. \quad (24)$$

Substituting (24) into (19) and then into (18) gives

$$\alpha = \begin{cases} nk \left[v^2 \left(\frac{f^2 + f - 1}{f + 1} \right) - \delta \right] \\ 0 \end{cases} \quad \text{if } nk \left[v^2 \left(\frac{f^2 + f - 1}{f + 1} \right) - \delta \right] < 0 \quad (25)$$

where $v = v_j/V_s$ and

$$\delta = 2gh_f/V_s^2. \quad (26)$$

If we take the effects of the steam evolution to be small then

$$f = \frac{\rho}{dP/dL} \sqrt{\frac{\rho}{\rho}} = \sqrt{\rho}. \quad (27)$$

With this value as an approximation, Eq. (25) can be solved iteratively allowing the integration of Eq. (16). It may be seen that Eqs. (20) and (28) abridge the usual penetration density law for hypervelocity target penetration, giving rise to a term that increases the effective density of the target material. Thus, in the case of impact activated materials the usual hypervelocity penetration density law differs from that appropriate for inert materials.

VI. DESIGN OPTIMIZATION FORMULATION FOR INFLUENCE ATTENUATION PANELS TO SUPPRESS SHELL - SHELL IMPACT JET INDUCED INITIATION

Assume a jet formed by the impact of two simultaneously initiated shells, as shown in Fig. 1, attacks an influence suppression structure of the kind shown in Fig. 2. Figure 5 illustrates the specific jet and suppressive structure concerned together with parameters representing the important dimensions and quantities. Assume the jet formed by the impact of the shells has an initial length ℓ of density ρ_0 , the density of the shell walls, and that subsequently the jet increases in length linearly with the difference between the jet tip velocity v_t and jet back velocity v_b . We assume also that the jet width increases from an initial value e with a velocity $\alpha v(x)$ where α is a constant equal to the angle of spread in jet material measured in radians and $v(x)$ is the forward velocity of the jet at any distance x along the initial jet length. The density of the jet is assumed to decrease inversely with the product of the fractional increase in width and local stretching in length.

We assume a linear velocity gradient given at any point x by

$$v = v_b + (v_t - v_b)x/\ell \quad (28)$$

where ℓ is the length of the jet at which the density is that of the steel. The time for material to reach any distance L will be referred to the time of initial jetting (virtual origin of the jet at $x=0$). Thus,

$$t(x) = L/v(x). \quad (29)$$

The jet element of length dx at x increases in length to dx' as of its arrival at L as given by

$$dx' = dx + t dv \quad (30)$$

Differentiating Eq. (28) to substitute for dv and using (29) to substitute for t in (30) gives on integrating

$$\begin{aligned} x' &= [1 + C_1 L / (1 + C_1 x)] dx \\ &= \ell + L \ln(1 + C_1 \ell) \end{aligned} \quad (31)$$

where

$$C_1 = (v_t - v_b) / \ell v_b. \quad (32)$$

This gives the length of the jet at any distance L from its origin.

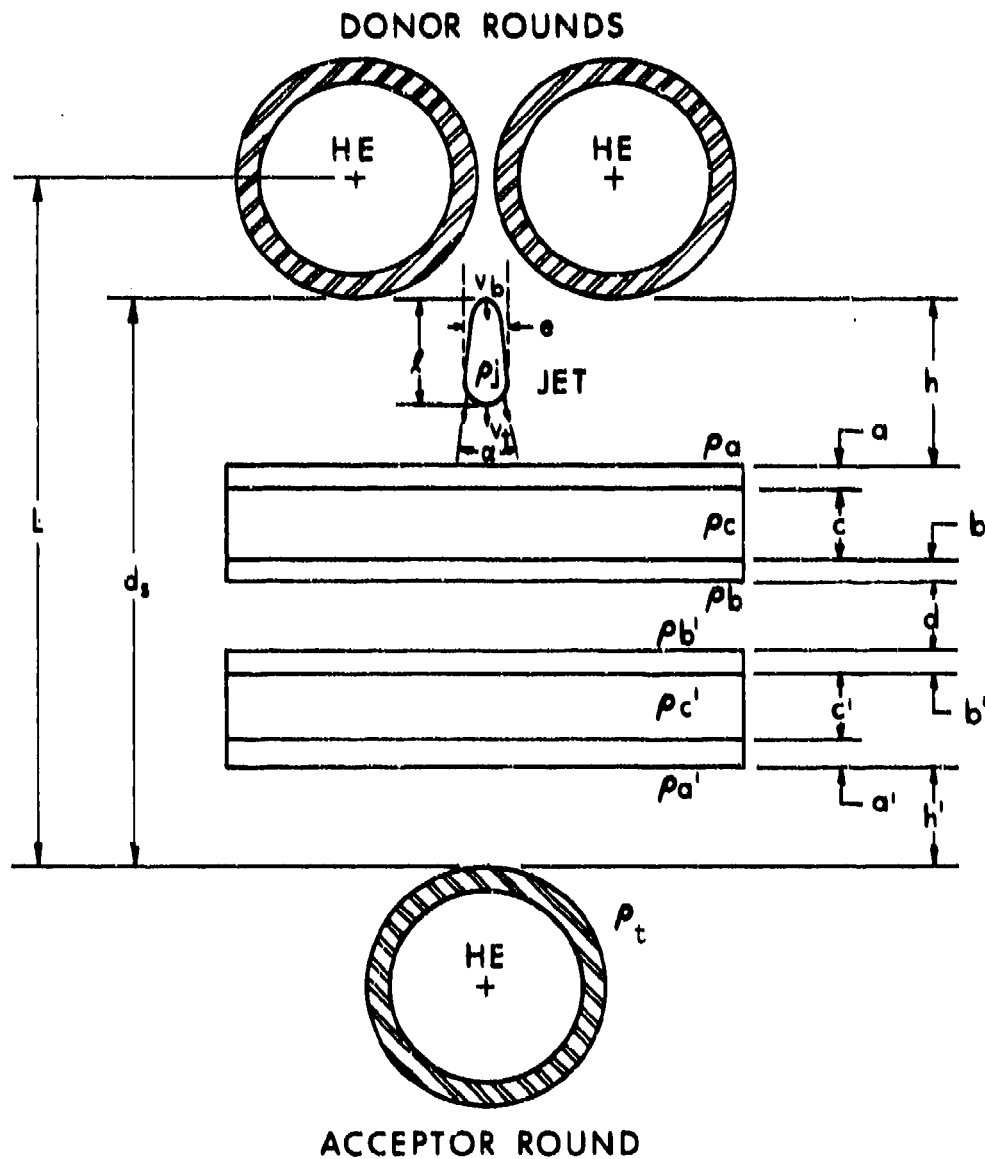


Figure 5. Schematic of the jet formed by simultaneously initiated artillery shells and antifraticide panels of the type shown in Fig. 2 defining the important parameters governing the interaction. Jet tip and base velocities v_t , v_b , width e , angular spread α , initial length l and jet density ρ_j , panel densities ρ_a , ρ_b , ρ_c , $\rho_{a'}$, $\rho_{b'}$, and $\rho_{c'}$, as well as the spatial configurational parameters, c' , h , d , d_s and L are shown. Density of the target is ρ_t .

The penetration of the unimpeded jet at L in a target (such as steel) of density ρ_t must be calculated in terms of the density of the jet as it arrives at the target. Since the jet initially forms a sheet of metal, its density drops as it expands laterally, i.e., normally to the surface of that sheet, and as it lengthens. Thus, we have for the density:

$$\begin{aligned}\rho_j(x,t) &= \rho_0 \frac{e}{e + \alpha v(x)t(x)} \left(\frac{dx'}{dx} \right)^{-1} \\ &= \rho_0 \left(1 + \frac{C_1 L}{1 + C_1 x} \right)^{-1} \frac{e}{e + \alpha vt}\end{aligned}\quad (33)$$

The penetration factor is $\sqrt{\rho_j/\rho_t}$. Thus, without influence suppression panels, the penetration P in the target at L will be

$$P = \int_0^L dx \sqrt{\rho_j/\rho_t} \left[1 + \frac{C_1(L + P(x))}{1 + C_1 x} \right] \quad (34)$$

where we have included the penetration into the target $L + P(x)$ as a correction to more accurately give the distance to the target. This correction is to be included in the expression for ρ_j as well, but only for the longitudinal extension of the jet:

$$\rho_j(x,t) = \rho_0 \left(1 + \frac{C_1(L + P(x))}{1 + C_1 x} \right)^{-1} \frac{e}{e + \alpha L} \quad (35)$$

This gives for the penetration into the target in the absence of suppressive layers:

$$P = \sqrt{\rho_0/\rho_t} \int_0^L dx \left(1 + \frac{C_1(L + P_x)}{1 + C_1 x} \right)^{1/2} / \left(1 + \frac{\alpha}{e} L \right)^{1/2} \quad (36)$$

where the notation P_x means

$$P_x \equiv P(x) = \sqrt{\rho_0/\rho_t} \int_0^x dx' \left(1 + \frac{C_1(L + P_x)}{1 + C_1 x'} \right)^{1/2} / \left(1 + \frac{\alpha}{e} L \right)^{1/2} \quad (37)$$

We now calculate the effects due to the presence of two suppressive structure panels through which the jet must pass before encountering the target plate. Assume panel 1 consists of the three layers of thickness a , c , and b as shown in Fig. 6. We have for the losses of jet length Δl_a ,

$\Delta l_c, \Delta l_b$

$$a = \sqrt{\rho_o/\rho_a} \int_{l-\Delta l_a}^l dx \left[1 + \frac{C_1(h + P_a)}{1 + C_1 x} \right]^{1/2} / \left(1 + \frac{\alpha}{\theta} h \right)^{1/2} \quad (38)$$

$$c = \sqrt{\rho_o/\rho_1} \int_{l-\Delta l_a-\Delta l_c}^{l-\Delta l_a} dx \left[1 + \frac{C_1(h+a+P_c)}{1 + C_1 x} \right]^{1/2} / \left[1 + \frac{\alpha}{\theta} (h + a) \right]^{1/2} \quad (39)$$

and

$$b = \sqrt{\rho_o/\rho_b} \int_{l-\Delta l_a-\Delta l_c-\Delta l_b}^{l-\Delta l_a-\Delta l_c} dx \left[1 + \frac{C_1(h+a+c+P_b)}{1 + C_1 x} \right]^{1/2} / \left[1 + \frac{\alpha}{\theta} (h+a+c) \right]^{1/2} \quad (40)$$

where P_a , P_c , and P_b are defined as the instantaneous penetration as in Eq. (37). The density ρ_1 is from (20), the "effective" value

$$\rho_1 = \rho_c (1 + \alpha) \quad (41)$$

For high velocity jet penetration, stagnation point temperatures are high, so that the efficiency η can be nearly unity. In this case (41) becomes

$$\rho_1 = \rho_c \left\{ 1 + k \left[v^2 \left(\frac{f^2 + f - 1}{f + 1} \right) - \delta \right] \right\} \quad (41a)$$

which is to be solved recursively. The total loss in length passing through panel 1 is therefore Δl_1 where

$$\Delta l_1 = \Delta l_a + \Delta l_c + \Delta l_b \quad (42)$$

During the jet's penetration of panel 1, a shock builds up in the jet as shown in Fig. 4. When the jet exits panel 1, the rarefaction wave from the newly formed free surface of the jet propagates into this region of high pressure, disrupting the jet material. Let us obtain an approximate expression for the loss of jet material due to this effect. There are two cases to be considered. First, if the penetration is supersonic an amount proportional (and approximately equal) to the jet thickness is lost, i.e., and amount ke_1 , where k is a proportionality constant approximately equal to unity. Since this should be expressed so that a zero thickness panel removes no jet material we will write for the loss length

$$y_1 = ke_1 / [1 + e_1 \rho_{j_1} / (a\rho_a + b\rho_b + c\rho_1)] \quad (43)$$

where e_1 is the jet width given in terms of the initial width by

$$e_1 = e / [1 + \frac{\alpha}{e} (h + a + b + c)] \quad (44)$$

and ρ_{j_1} is the density of the jet on exit from the first panel. In this length y_1 , shocks of pressure p_1 given by

$$p_1 = \frac{\rho_1 \rho_{j_1}}{2(\sqrt{\rho_1} + \sqrt{\rho_{j_1}})^2} v_1^2 \quad (45)$$

where ρ_1 should be taken to be the average density within a mass column equal to $e_1 y_1$, act on the mass column. In essence this means $\rho_1 = \rho_b$ unless $b \ll e$ or $\rho_b \ll \rho_j$. Also, ρ_{j_1} should be taken to be the jet density at exit from panel 1:

$$\rho_{j_1} = \rho_0 \left(1 + \frac{C_1(h+a+b+c)}{1+C_1(l-\Delta l_1)} \right)^{-1} \frac{e}{e+\alpha(l-\Delta l_1)} \quad (46)$$

Here v_1 is the corresponding velocity at $x = l - \Delta l_1$ as given by Eq. (38). Now the pressure p_1 causes the jet to spread laterally and thus drop in effectiveness against the next plate. This loss in effective length Δy_1 is calculated from density considerations to be

$$\Delta y_1 = -y_1 [1 - \sqrt{(1 + \alpha d/e) / (1 + \alpha f_1 d/e)}] \quad (47)$$

where

$$f_1 = \frac{\alpha v_1}{\alpha v_1 + (p_1 / \rho_{j_1})^{1/2}} \quad (48)$$

In the case of subsonic penetration of the panel, the shock zone in the jet will increase with penetration distance. However, the strength of the shock will decrease. Thus, Eq. (47) will serve as an approximation of the jet length loss in that case as well. This length loss is equivalent to an initial length decrement $\Delta l_1'$ given by

$$\Delta y_1 = \int_{\ell - (\Delta \ell_1 + \Delta \ell_1')}^{\ell - \Delta \ell_1} dx \left[1 + \frac{C_1 (h + a + b + c + d)}{1 + C_1 x} \right] \quad (49)$$

At panel 2 the length loss is to be computed in the same fashion as for the first panel. We have in the appropriate order:

$$b' = \sqrt{\rho_0 / \rho_{b'}} \int_{\ell - (\Delta \ell_1 + \Delta \ell_1') - \Delta \ell_{b'}}^{\ell - (\Delta \ell_1 + \Delta \ell_1')} dx \left[1 + \frac{C_1 (L_2 + p_{b'})}{1 + C_1 x} \right]^{1/2} / \left[1 + \frac{\alpha}{e} L_2 \right]^{1/2} \quad (50)$$

where

$$L_2 = h + a + b + c + d \quad (51)$$

$$c' = \sqrt{\rho_0 / \rho_2} \int_{\ell - (\Delta \ell_1 + \Delta \ell_1') - \Delta \ell_{b'} - \Delta \ell_{c'}}^{\ell - (\Delta \ell_1 + \Delta \ell_1') - \Delta \ell_{b'}} dx \left[1 + \frac{C_1 (L_2 + b' + p_{c'})}{1 + C_1 x} \right]^{1/2} / \left[1 + \frac{\alpha}{e} (L_2 + b') \right]^{1/2} \quad (52)$$

and

$$a' = \sqrt{\rho_0 / \rho_{a'}} \int_{\ell - (\Delta \ell_1 + \Delta \ell_1') - \Delta \ell_2}^{\ell - (\Delta \ell_1 + \Delta \ell_1') - \Delta \ell_{b'} - \Delta \ell_{c'}} dx \left[1 + \frac{C_1 (L_2 + b' + c' + p_{a'})}{1 + C_1 x} \right]^{1/2} / \left[1 + \frac{\alpha}{e} (L_2 + b' + c') \right]^{1/2} \quad (53)$$

where

$$\Delta \ell_2 = \Delta \ell_{a'} + \Delta \ell_{b'} + \Delta \ell_{c'} \quad (54)$$

As in the case for Eq. (41), we write for ρ_2

$$\rho_2 = \rho_{c'} (1 + \alpha') = \rho_{c'} \left\{ 1 + k \left[v^2 \frac{f^2 + f - 1}{f + 1} - \delta \right] \right\} \quad (55)$$

Again we calculate the effective loss in jet length due to shocks in the jet on exit from the second panel. Corresponding to Eq. (43) to (49) we have

$$y_2 = k e_2 / [1 + e_2 \rho_{j2} / (a' \rho_{a'} + b' \rho_{b'} + c' \rho_{c'})] \quad (56)$$

with

$$e_2 = e / [1 + \frac{\alpha}{e} (L_2 + a' + b' + c')]. \quad (57)$$

The shock pressure p_2 is

$$p_2 = \frac{\rho_2 \rho_{j_2}}{2(\sqrt{\rho_2} + \sqrt{\rho_{j_2}})^2} v_2^2 \quad (58)$$

where

$$\rho_{j_2} = \rho_0 \left(1 + \frac{C_1(L_2 + a' + b' + c')}{1 + C_1(\ell - \Delta\ell_1 - \Delta\ell_1' - \Delta\ell_2)} \right)^{-1} \frac{e}{e + \alpha(\ell - \Delta\ell_1 - \Delta\ell_1' - \Delta\ell_2)} \quad (59)$$

and v_2 is the velocity at $x = \ell - \Delta\ell_1 - \Delta\ell_1' - \Delta\ell_2$ as given by Eq. (38). The spread in the jet produces the effective loss

$$\Delta y_2 = -y_2 [1 - \sqrt{(1 + \alpha h'/e)/(1 + \alpha f' h'/e)}] \quad (60)$$

where

$$f' = \frac{\alpha v_2}{\alpha v_2 + (p_2/\rho_{j_2})^{1/2}} \quad (61)$$

Therefore, $\Delta\ell_2'$, the effective loss in initial rod length due to the gap h' is

$$\Delta y_2 = \int_{\ell - (\Delta\ell_1 + \Delta\ell_1') - \Delta\ell_2 + \Delta\ell_2'}^{\ell - (\Delta\ell_1 + \Delta\ell_1') - \Delta\ell_2} dx \left[1 + \frac{C_1(L_2 + a' + b' + c' + h')}{1 + C_1 x} \right] \quad (62)$$

Finally, the remaining rod material penetrates into the target a distance

$$p' = \sqrt{\frac{\rho_0}{\rho_t}} \int_0^{\ell - (\Delta\ell_1 + \Delta\ell_1') - (\Delta\ell_2 + \Delta\ell_2')} dx \left[1 + \frac{C_1(L + p' x)}{1 + C_1 x} \right]^{1/2} / \left(1 + \frac{\alpha}{e} L \right)^{1/2} \quad (63)$$

VII. COMPUTATIONS

A computer code designated "Main" to compute P' has been developed and is given in Appendix A. This code has been used to compute shield effectiveness curves. The effectiveness of a single homogeneous panel to suppress jet induced influence is shown in Figs. 6-9. The nondimensional penetration (in units of donor round radius) P' as a function of the nondimensional panel thickness (also in units of donor round radius) is plotted for the case of separation distance d_s equal to 1.0 R (Fig. 6), 2.0 R (Fig. 7), 3.0 R (Fig. 8), and 4.0 R (Fig. 9). The shield panel is taken to be equidistant between the donor and acceptor rounds. Panel density ρ_c is taken as a parameter for Figs. 6-9. Values of specific parameters have been taken to provide an optimum fit to experimental data obtained from pipe bomb tests as discussed below.⁴ X-rays made during these pipe bomb tests were employed to obtain the jet characteristic parameters' values. Specific values used are:

Jet Characteristics: $\rho_o = 8.0 \text{ g/cm}^3$

$$l = 0.2$$

$$e = 0.4$$

$$\alpha = 0.1$$

$$v_t = 2.0 \text{ km/s}$$

$$v_b = 0.5 \text{ km/s}$$

Target: $\rho_t = 8.0 \text{ g/cm}^3$

Other: $k = 2.0$

$$v_s = 3.0 \text{ km/s}$$

$$g = 0.0 \text{ and } 0.209$$

The results obtained for the two values of g were nearly the same. The values of jet characteristic parameters are dependent on the donor rounds used. For rounds that do not scale to the approximate values of the pipe bombs used in Ref. 4, scaling test should be made before the results of Figs. 6-9 are used for applications. The curves offer no surprises, but simply show that increased thickness and increased density both decrease monotonically the penetration in an acceptor round. The curves can be used to obtain the requirements to just stop a jet from penetrating into the acceptor.

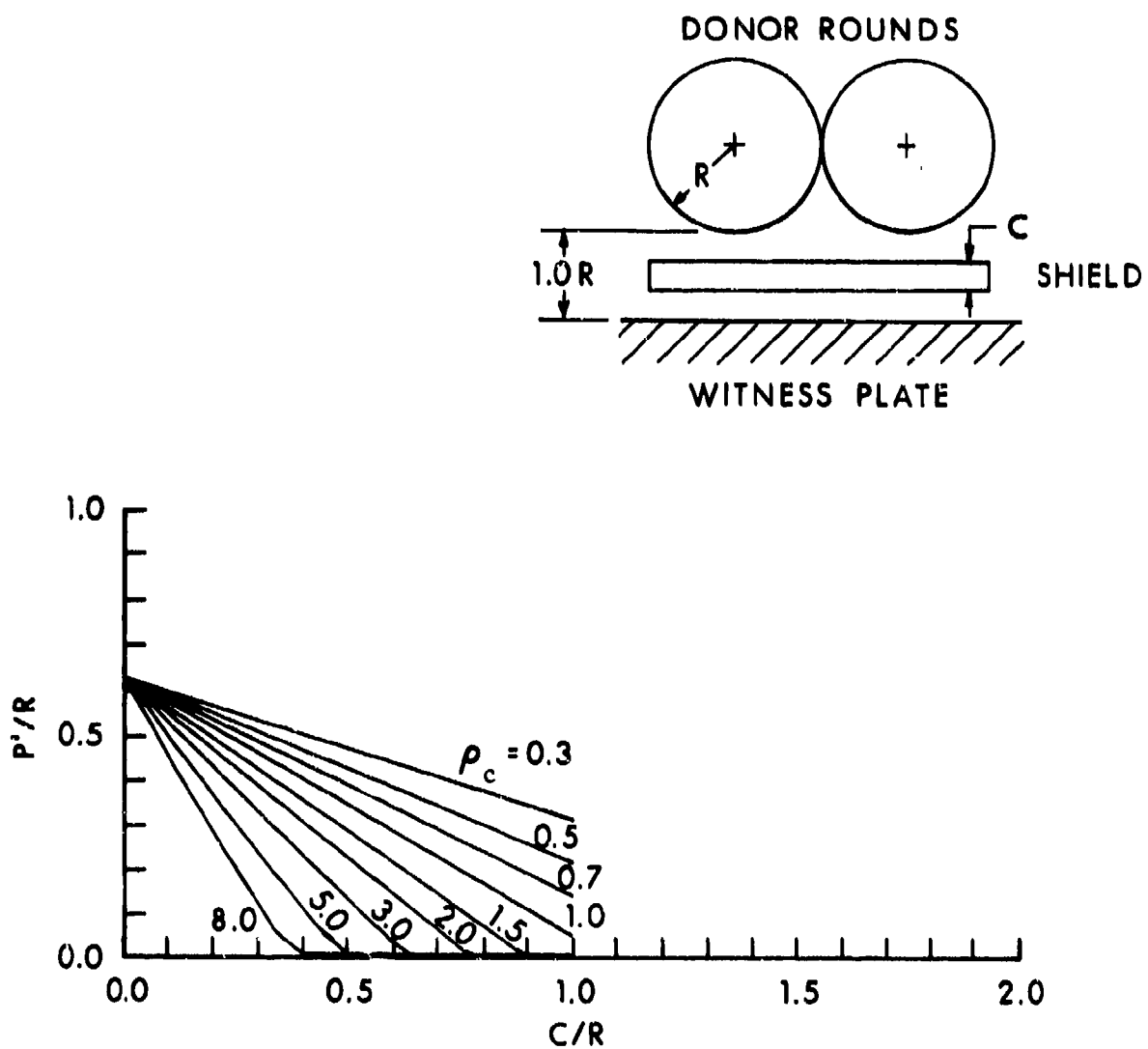


Figure 6. Nondimensional penetration P'/R versus nondimensional shield thickness C/R , where shield is placed at midpoint between donor and acceptor rounds (or witness plate, as shown in inset) separated by $1.0 R$. Shield density ρ_c is parameter for the family of curves.

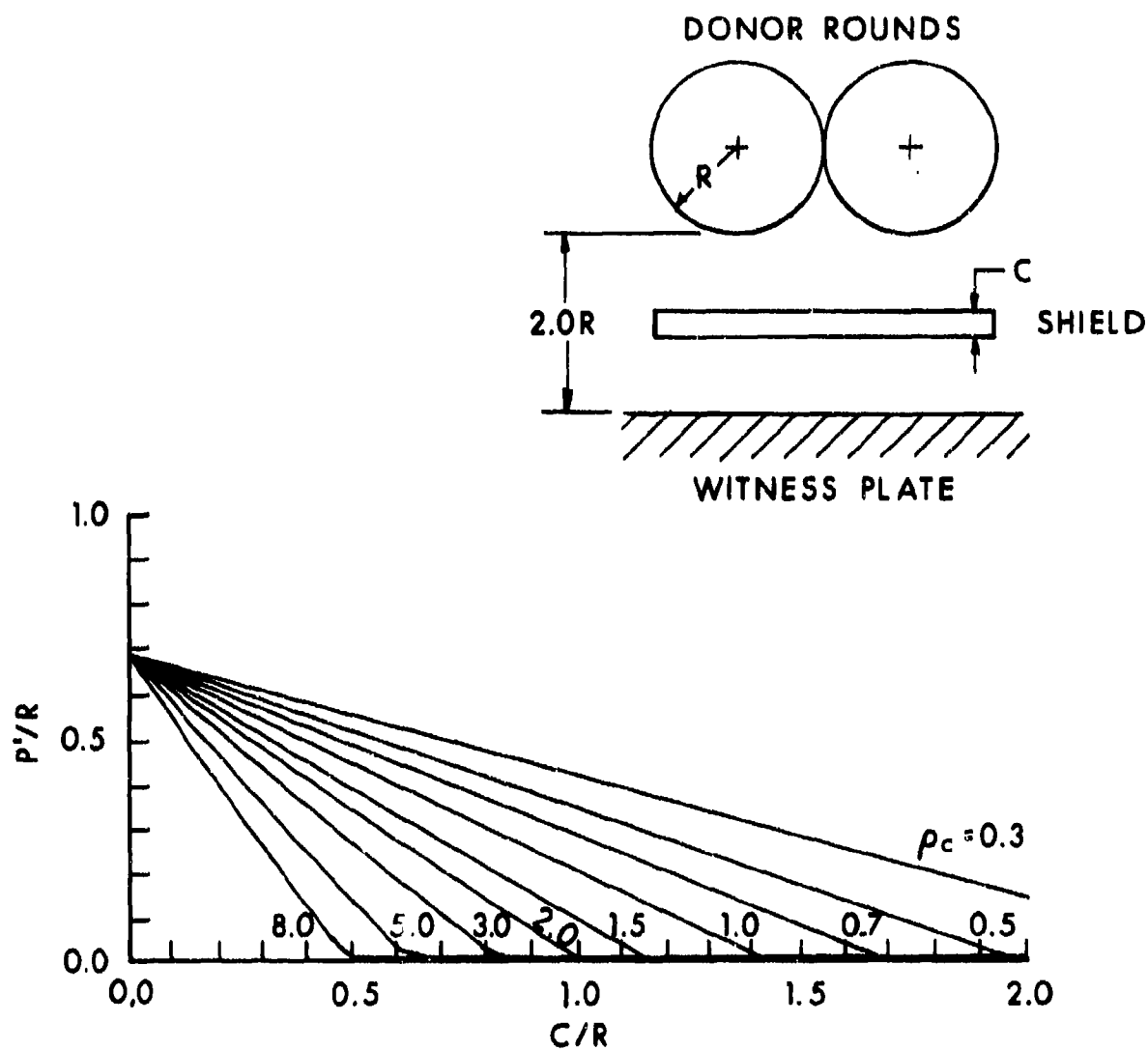


Figure 7. Nondimensional penetration P'/R versus nondimensional shield thickness C/R , where shield is placed at midpoint between donor and acceptor rounds separated by $2.0 R$. Shield density ρ_c is a parameter for the family of curves.

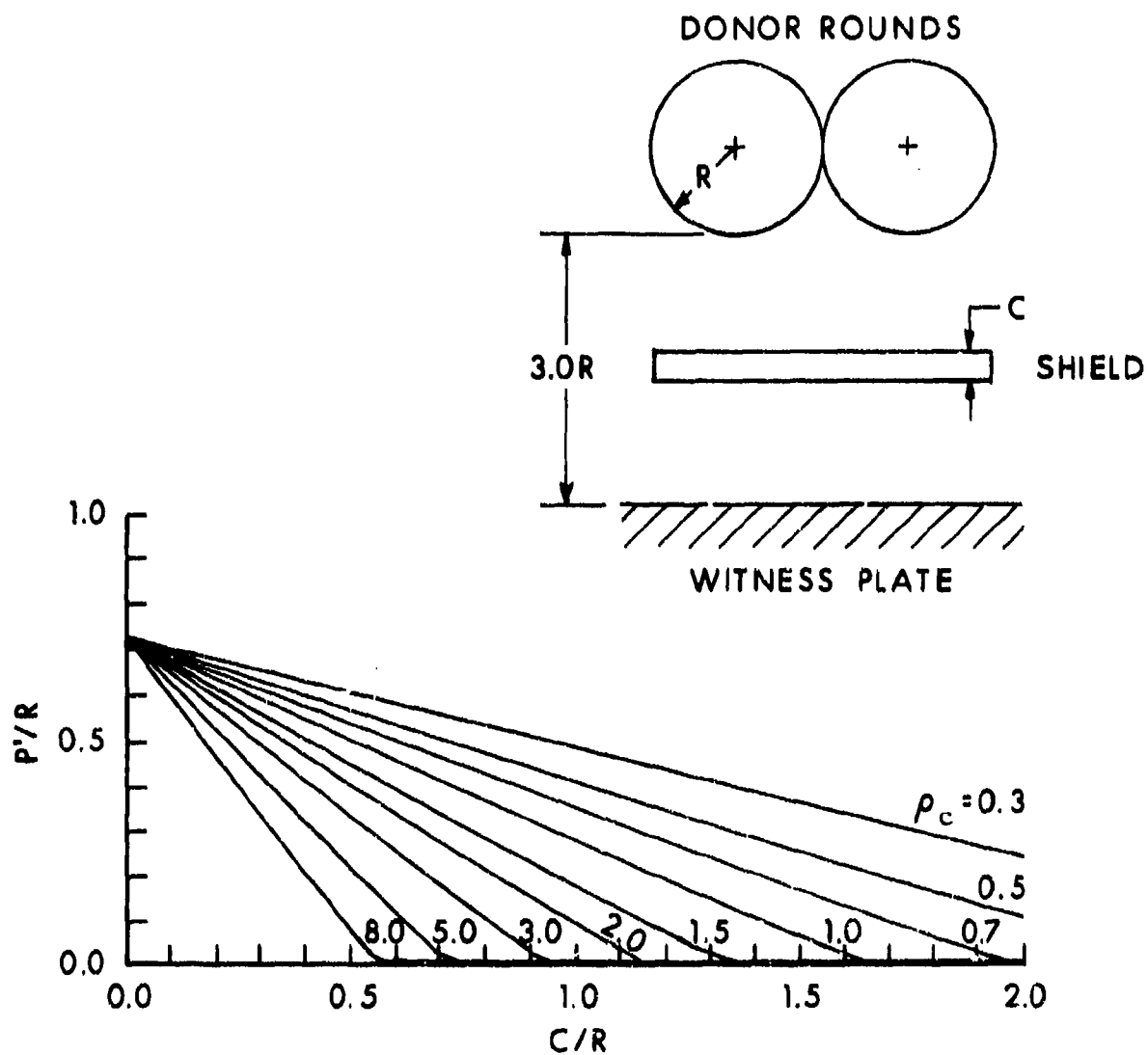


Figure 8. Nondimensional penetration P'/R versus nondimensional shield thickness C/R , where shield is placed at midpoint between donor and acceptor rounds separated by $3.0 R$. Shield density ρ_c is parameter for the family of curves.

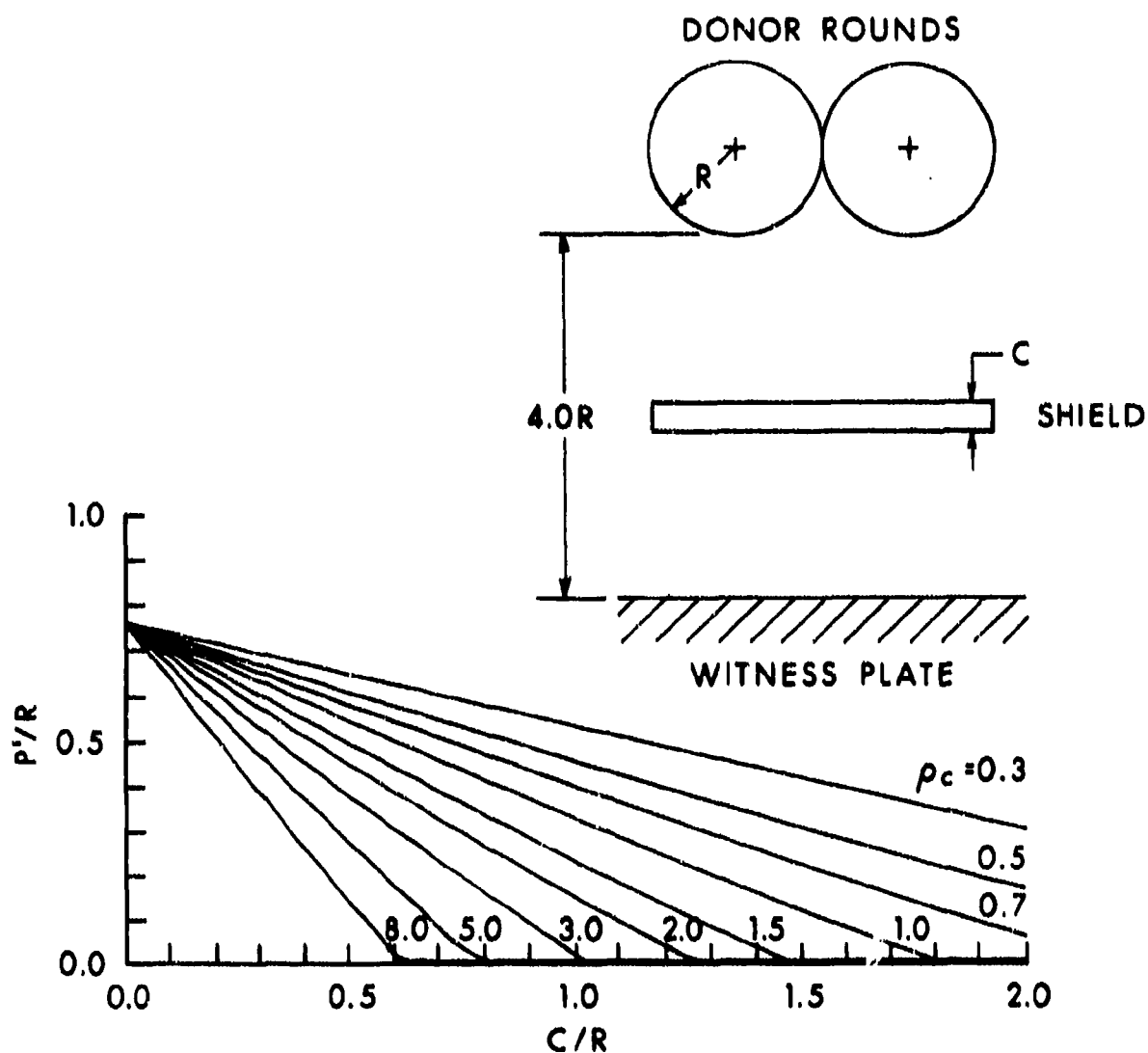


Figure 9. Nondimensional penetration P'/R versus nondimensional shield thickness C/R , where shield is placed at midpoint between donor and acceptor rounds separated by $4.0R$. Shield density ρ_c is parameter for the family of curves.

Figure 10 shows the results obtained for the nondimensional penetration depth as a function of the separation distance D/R for two panels placed symmetrically about the midpoint between the donor and acceptor (or target) rounds. The result is obtained for several densities and for panels 0.53 R thick (this corresponds to panels 1/2" or 1.27 cm thick in the pipe bomb experiments). Separation between donor and acceptor rounds is taken to be 4.0 R in these calculations. These curves show that the penetration versus separation distance drops as the separation increases. This is easily understood as an effect of jet elongation with travel distance. As a result, it is concluded that for a fixed amount of buffer material it is better to separate the material into two panels placed close to or against the shells. Figures 11-14 incorporate the optimum shield material distribution, i.e., separation of the shield material, into two panels as indicated by the results shown in Fig. 10. Comparison with Figs. 6-9 shows the improvement afforded by such an arrangement of shield material. Note that the curves in Figs. 6-9 give the same value at zero total shield thickness and for shields completely filling the donor-acceptor round gap as the corresponding curves in Figs. 11-14. At points in between, however, the curves in Figs. 11-14 dip below their counterparts in Figs. 6-9. These results show that the improvement noted in Fig. 10 as to the optimum placement of shield material under the symmetry constraint is general.

Figure 15 gives data showing that a further improvement in buffer material efficiency is achieved using a "foam" (a low density material) filling the gap between the shells. The curve gives the penetration as a function of the density of the "foam" buffer filling the entire gap. It is seen that the penetration in the target plate is zero at a density of about 0.21 g/cm³ for a gap of 4.0R. This is equivalent to a 1.05 R thick panel of density 0.80 g/cm³ which placed at the midpoint will not protect the target plate (penetration $P'/R=0.15$); divided into two 0.525 R thick panels the penetration is $P'/R=0.13$. Therefore, the best panel design appears to be a low density "foam" filling the available gap.

VIII. COMPARISON WITH EXPERIMENTAL RESULTS

An extensive series of shield tests using 4.82 cm (1.9") diameter pipe bombs has been run employing a wide variety of shields. The data obtained in these tests has been used to validate the "Main" code. Figure 16 shows a comparison between the experimental and theoretical code results. In Fig. 16 the penetration depth (maximum depth in the target plate) is used for the ordinate while the individual test code numbers (these are the same code numbers used to designate the tests in Ref. 4) are listed along the abscissa. The order of the tests listed along the abscissa is not important. As listed, however, they imply a decreasing function of penetration with increasing shield material. Beneath each entry is a small picture indicating the test arrangement of the shield along with the shield thickness in mm together with symbols indicating shield materials used. Additional test details may be found in Ref. 4. All tests employed Comp B filled 4.82 cm diameter pipe bombs 15 cm in length placed 4 radii above a steel witness plate. The reference case shows the results for no shield between the two pipe bombs and the witness plate. The error bars (obtained from the test data for three shots) indicate the considerable variability of the results obtained in these tests.

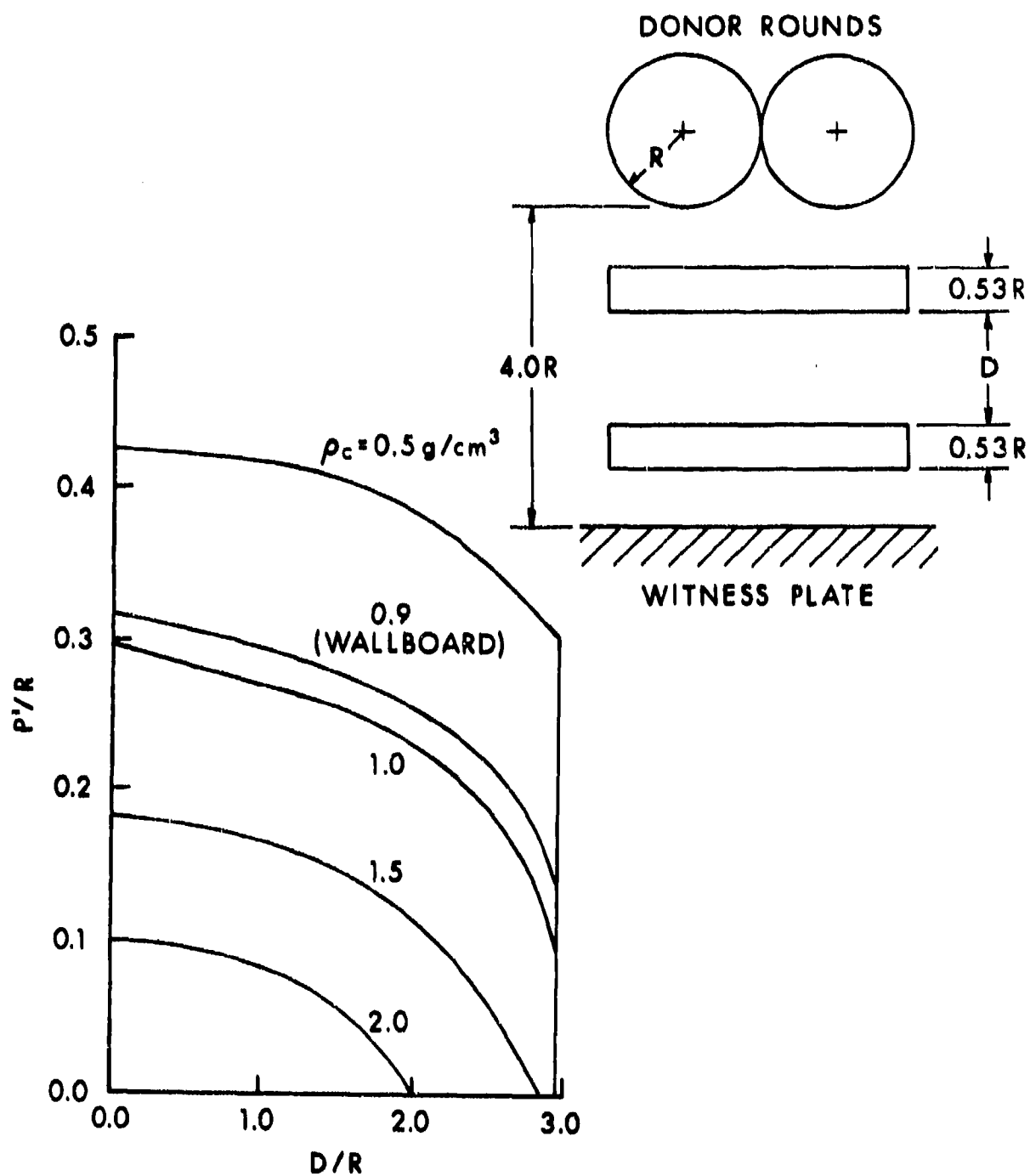


Figure 10. Nondimensional penetration P'/R versus nondimensional panel separation distance D/R for two symmetrically placed $0.53 R$ thick panels in a $4.0 R$ space between donors and target plate for various panel densities. The inset shows the geometry. These results indicate that if symmetry must be maintained in packaging, the best placement of shield material is midway between donor and acceptor rounds.

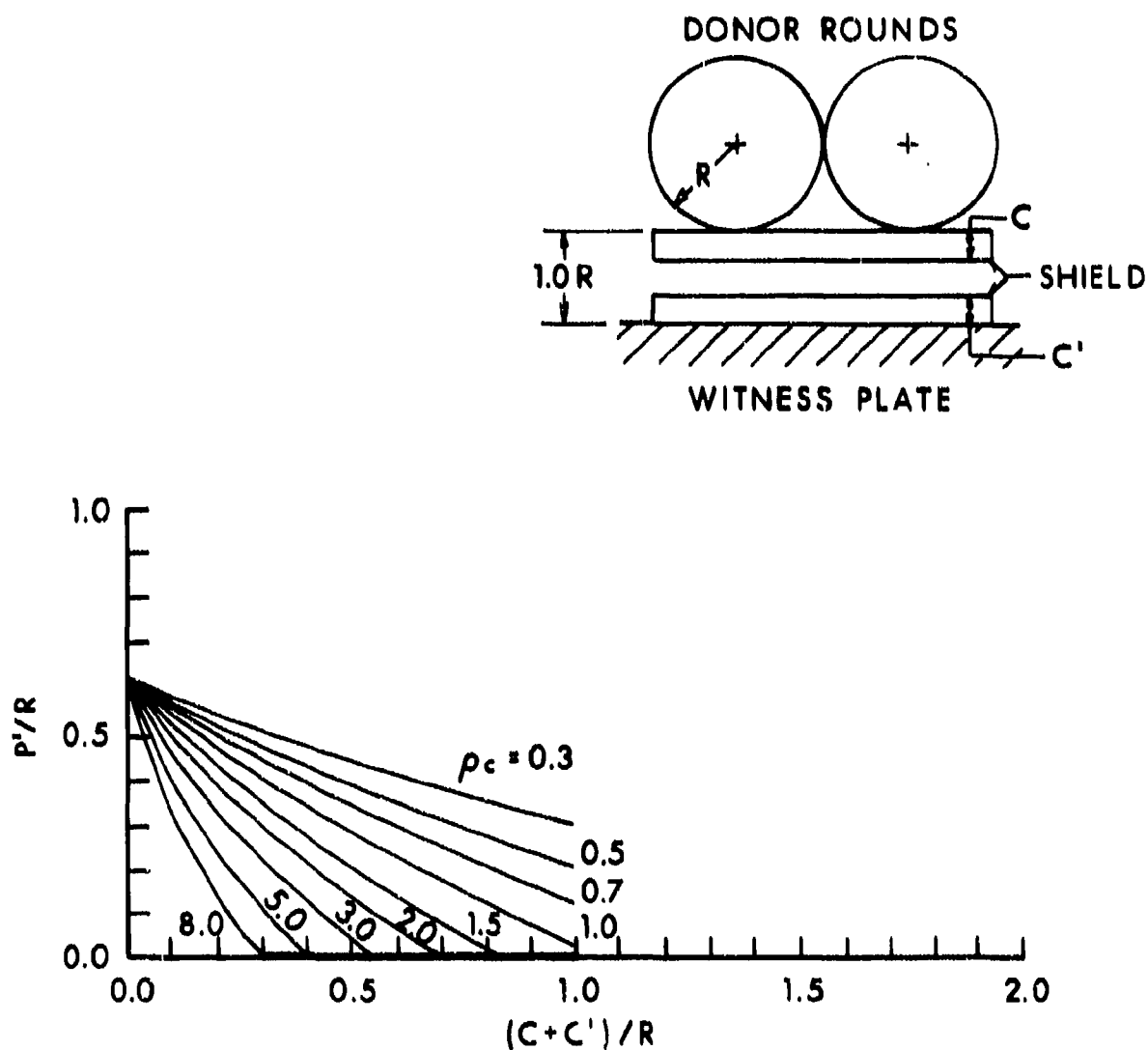


Figure 11. Nondimensional penetration P'/R versus nondimensional total shield thickness $(C + C')/R$, where the shield consists of two panels symmetrically placed about the midpoint, one against the donor rounds, one against the acceptor rounds (or witness plate, as shown in the inset). Donor-acceptor separation is $1.0 R$. Shield density ρ_c is parameter for curves.

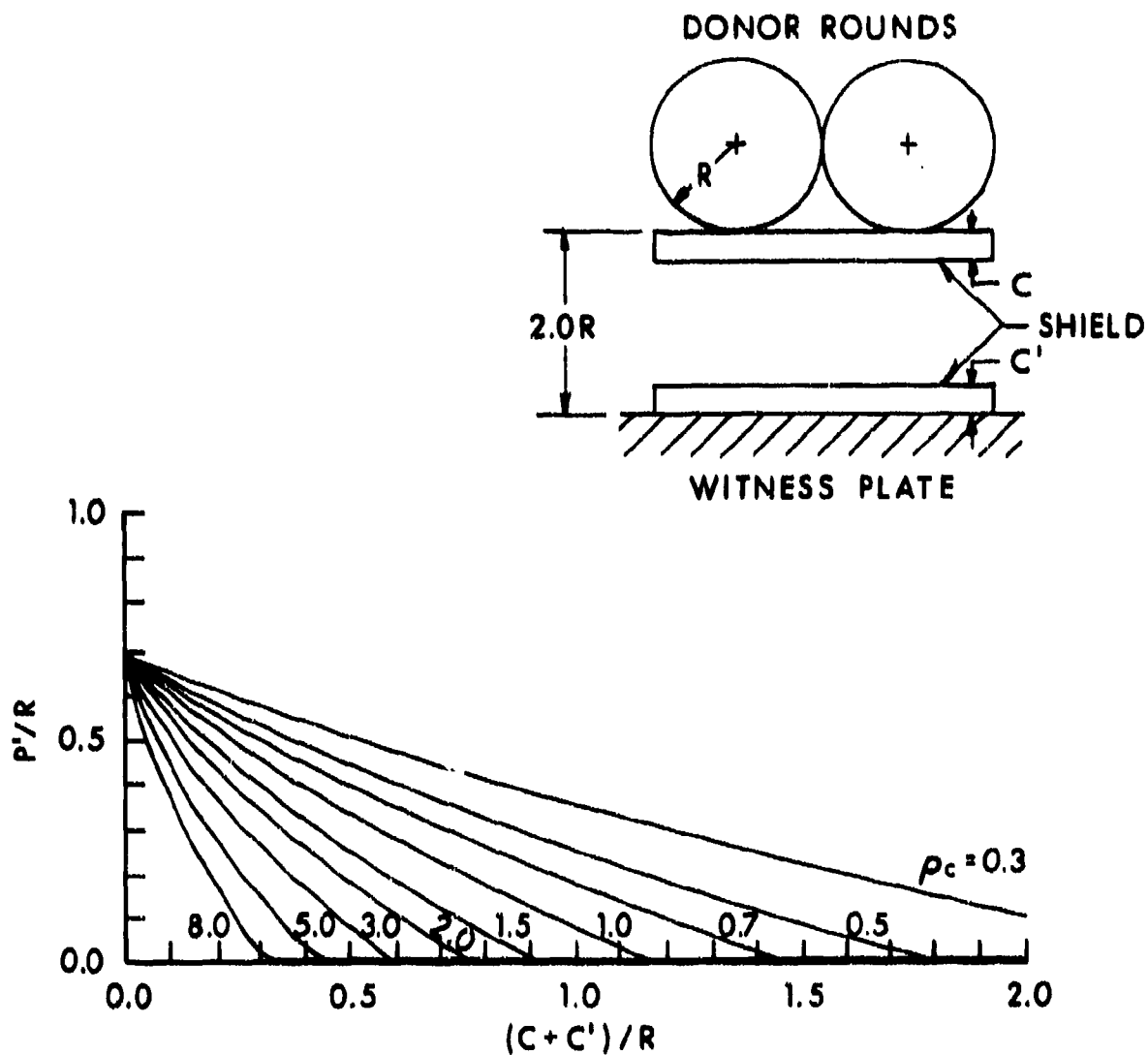


Figure 12. Nondimensional penetration P'/R versus nondimensional total shield thickness $(C + C')/R$, where the shield consists of two panels symmetrically placed about the midpoint, one against the donor rounds, one against the acceptor rounds (or witness plate as shown in inset). Donor-acceptor separation is $2.0 R$. Shield density ρ_c is parameter for curves.

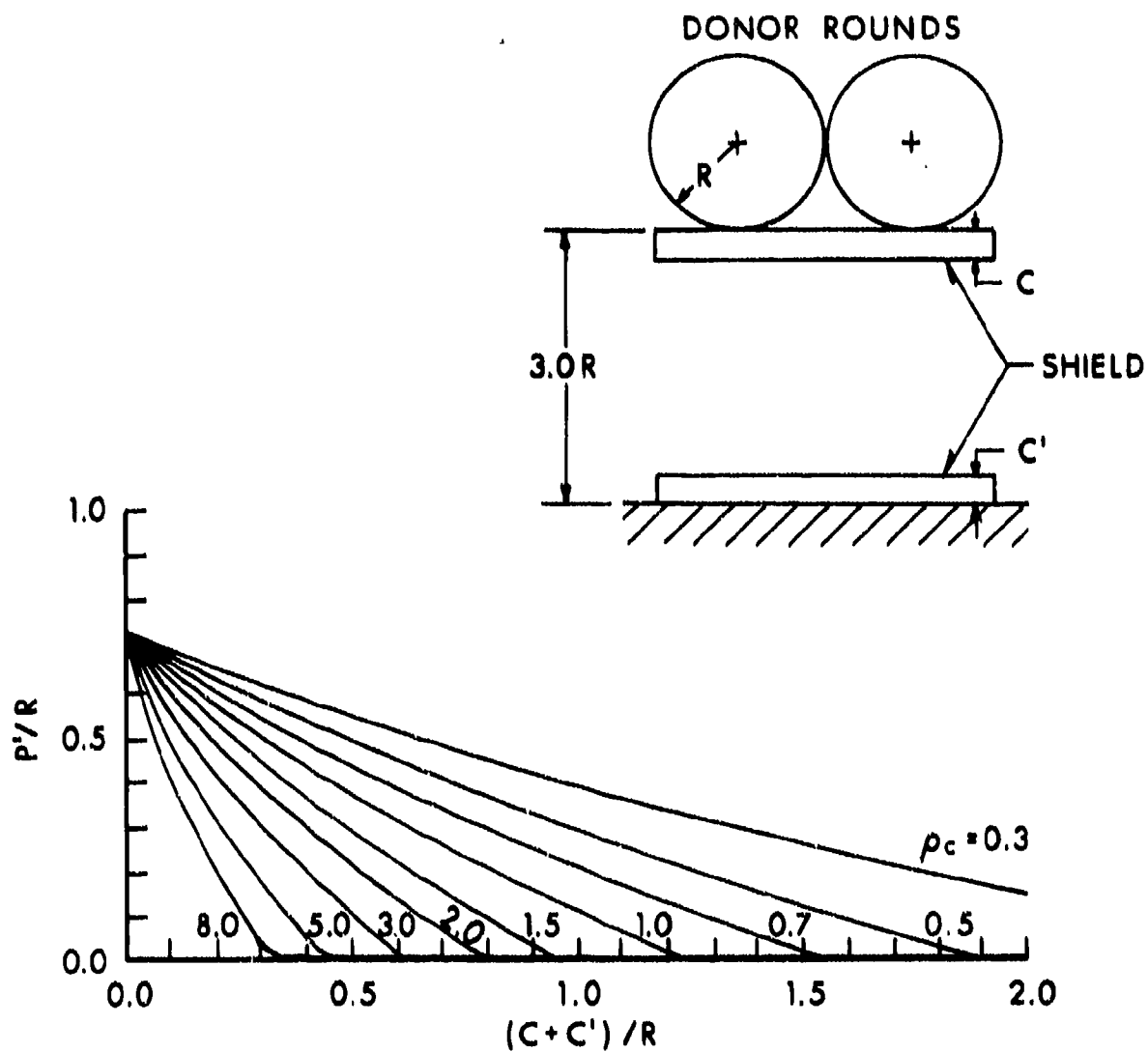


Figure 13. Nondimensional penetration P'/R versus nondimensional total shield thickness $(C + C')/R$, where the shield consists of two panels symmetrically placed about the midpoint, one against the donor rounds, one against the acceptor rounds (or witness plate, as shown in inset). Donor-acceptor separation is $3.0 R$. Shield density ρ_c is parameter for curves.

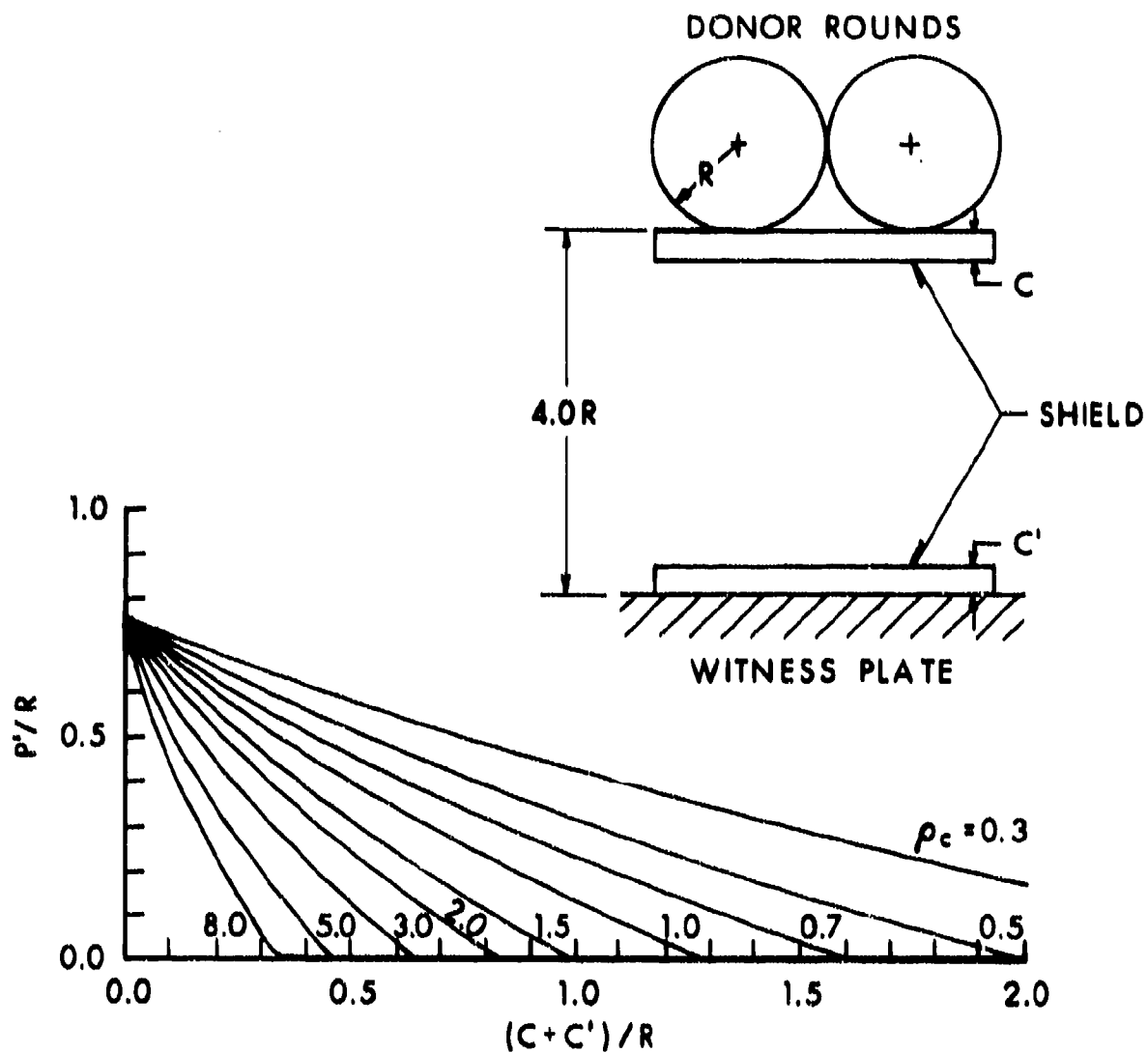


Figure 14. Nondimensional penetration P'/R versus nondimensional total shield thickness $(C + C')/R$, where the shield consists of two panels symmetrically placed about the midpoint, one against the donor rounds, one against the acceptor rounds (or witness plate as shown in inset). Donor-acceptor separation is $4.0 R$. Shield density ρ_c is parameter for curves.

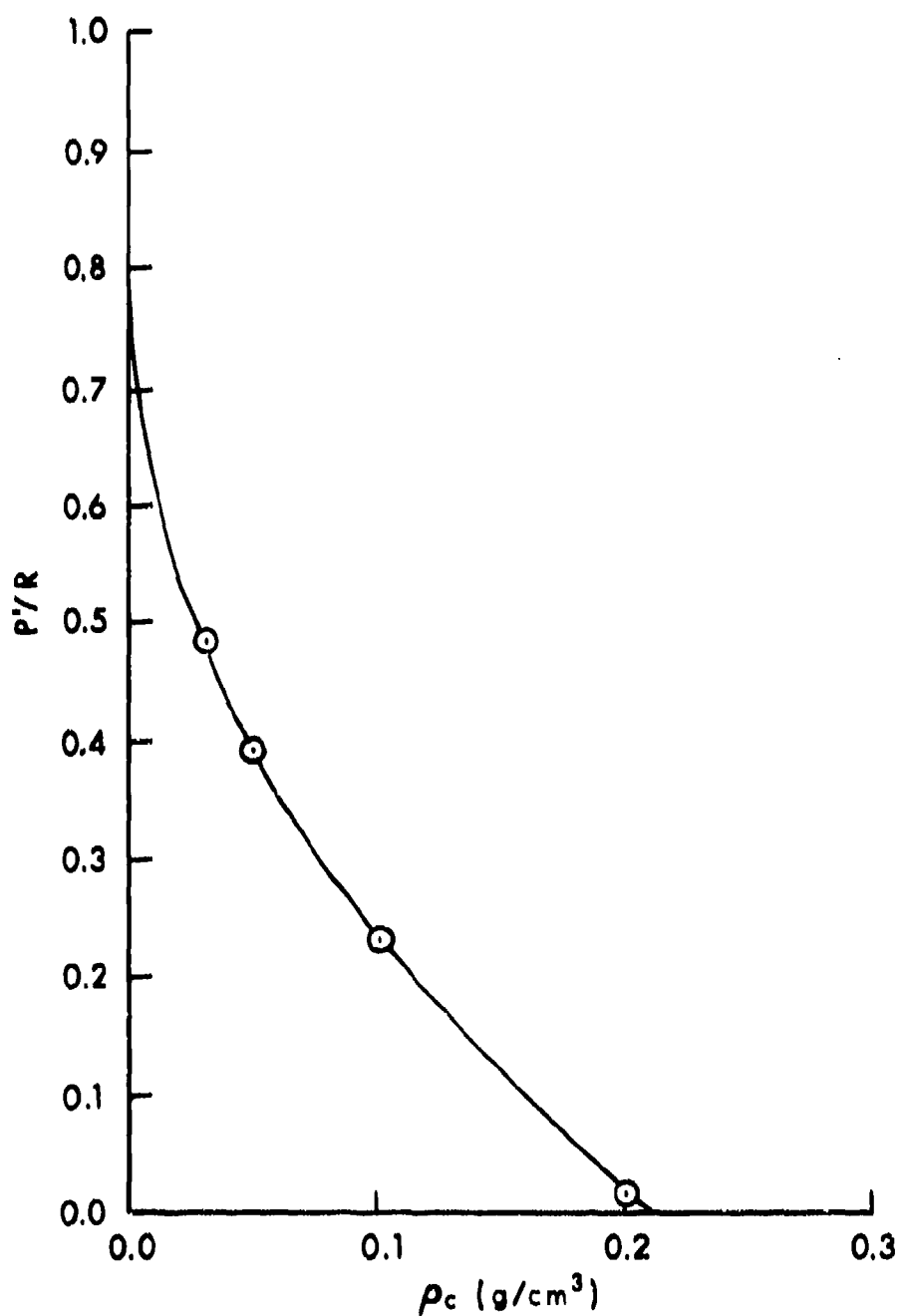


Figure 15. Nondimensional penetration versus density of shield material for a "foam" filling the space between the donor rounds and target plate (acceptor rounds) for a gap of 4.0 R.

☒ EXPERIMENTAL DATA
☒ THEORETICAL DATA
AND NO DETONATION
D DETONATION

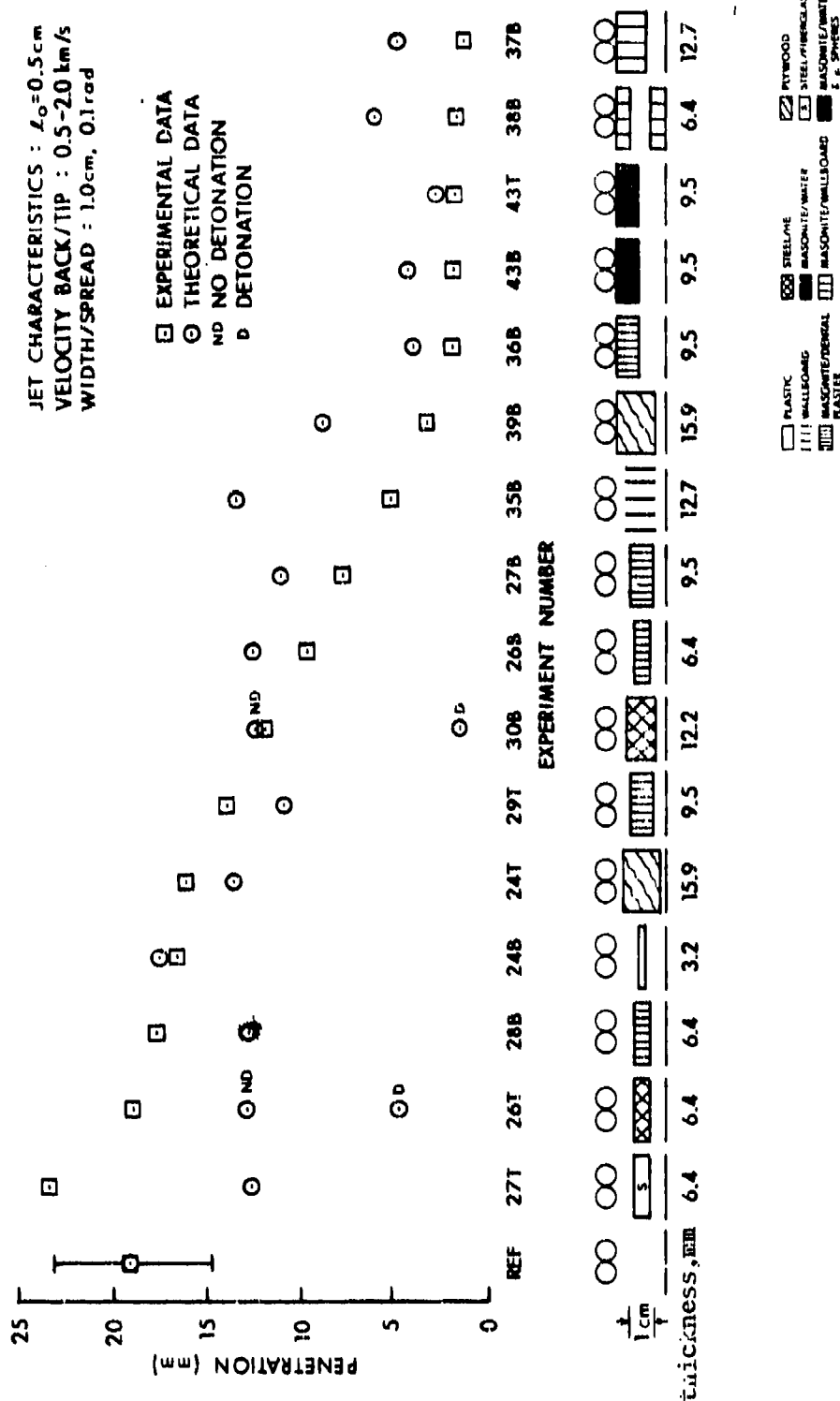


Figure 16. Penetration depth in mm charted for the several experimental shield tests. Theoretical and experimental data points have been plotted for all pipe bomb tests having bombs in contact 4.0 R above the witness plate. Schematics of each test shot with shield thickness, position and composition notes are shown below shot number. Note the error bars on the reference (no shield) test indicating the variability of the test results. Within these limits agreement between the experimental and theoretical results is good. Note also that the data trend is an artifact of the ordering of test shot data. As expected from theory, the smallest penetrations occurred for shields placed against donor rounds.

In tests 26T and 30B Detasheet was employed between thin sheets of steel to form the shield. The code computed shielding assuming both detonation of the Detasheet and no detonation. The results assuming no detonation are seen to agree satisfactorily with the observed results. At the right side of Fig. 16 are located all the tests in which a shield panel is placed against the donor rounds. It will be noticed that these six tests yielded the best shielding (least penetration into the witness plate) results. This is in general agreement with the predictions of the code as indicated by the results in Fig. 10. Overall the theoretical results given by the code correspond well with the experimental results in Fig. 16. (The reader should keep in mind that in some cases the penetration data is a measurement taken for two or three fragment craters in the witness plate that may be no more than 2-3 mm in diameter.) The experimental data must be regarded as having significant error bars reflecting the variability of these test results. Within these limitations, therefore, the model works well.

The results obtained in matching the experimental and theoretical data indicated that the effects observed were due to the mass column of shield material, and placement of that material alone. The code indicated no significant effect due to the use of hydrates in the shield. Several shots to test this hypothesis have been carried out by G. Gibbons⁴. In these shots equal mass columns of steel, aluminum, plaster, and water were used as shields. Damage to the witness plates was almost identical in these four shots, although in the shot using steel for the shield, the shield material itself produced some pitting in the witness plate (these pits were located to either side of the area usually damaged by the jet from the donor rounds).

IX. CONCLUSIONS

If two neighboring artillery shells in an ammunition pallet are simultaneously detonated, a high velocity metal jet is formed that can detonate other neighboring shells, even if these shells are protected by a significant thickness of armor (for example 15 cm of armor can be penetrated by the jet from two simultaneously detonated 155 mm HE artillery rounds). Equations to model the interaction of shield panels with such jets have been derived and employed to write a computer code to calculate penetration depth of the jet after passing through up to two panels consisting of sandwiches of up to three layers of material. In the code one layer in each panel (the middle layer in three layer panels) can consist of an explosive or a hydrated material that may be activated to yield enhanced pressures under the shock loading of the jet.

Computations using the code have indicated:

(1) The primary effect produced by inert or hydrated materials depends on the mass column of material in the panel and panel placement. Water of hydration produces only minor effects.

(2) The optimum placement for the shield panel to suppress jets is against the donor shells.

(3) Under symmetry requirements (i.e., where all shells must be equally shielded) the best placement employs two shields of equal thickness, one against the donor, one against the acceptor rounds.

(4) Use of explosive material sandwiched in the shields can significantly enhance the effectiveness of the shields. (Such material, however, may enhance impact shock initiation,)

(5) The best symmetric shield design (minimum weight basis) for inhibiting fratricide jets would employ a single panel filling the entire available space between donor and acceptor rounds with the lowest density material capable of inhibiting the jet (as given by the curves in Figs. 6-9) in the available space.

ACKNOWLEDGEMENTS

I would like to thank Gould Gibbons, Jr. of the EEB, TBD for furnishing much of the data used to compare the theoretical calculations with experimental results. I would also like to thank Toni Dorsey for extensive assistance in developing and exercising the computer code "Main." Finally, I wish to acknowledge Dr. Philip M. Howe for proposing this research problem and for his constructive suggestions regarding this task.

APPENDIX

PROGRAM "MAIN"

PROGRAM MAIN(INPUT,OUTPUT,TAPE5=INPUT,TAPE6=OUTPUT,TAPE9)	MAIN	2
DIMENSION GG(20), JD(20), RRHO(20)	MAIN	3
DIMENSION LAB(4), PLC(50), PLPP(50)	MAIN	4
C *** FORMATS	MAIN	5
C	MAIN	6
1 FORMAT(' GAP =',E11.4,')	MAIN	7
2 FORMAT(3X,'ICC = ',I10,4X,'PLC =',E11.4,3X,'PLPP =',E11.4,')	MAIN	8
4 FORMAT(A10)	MAIN	9
5 FORMAT(A10,10X,'LL =',I5)	MAIN	10
10 FORMAT(1H1)	MAIN	11
15 FORMAT(1H0)	MAIN	12
20 FORMAT(8E10.3)	MAIN	13
25 FORMAT(I5)	MAIN	14
30 FORMAT(4X,'A =',E11.4,6X,'B =',E11.4,3X,'BP =',E11.4,5X,'AP =',E11	MAIN	15
1.4,6X,'C =',E11.4,5X,'CP =',E11.4,/,4X,'D =',E11.4,' RADIUS =',E11	MAIN	16
2.4,6X,'H =',E11.4,3X,'HP =',E11.4,5X,'AL =',E11.4,3X,'RHOZ =',E11.	MAIN	17
34,/,4X,'E =',E11.4,5X,'VT =',E11.4,5X,'VB =',E11.4,2X,'ALPHA =',E1	MAIN	18
41.4,3X,'RHOT =',E11.4,3X,'RHOA =',E11.4,/,1X,'RHOB =',E11.4,3X,'RH	MAIN	19
50C =',E11.4,2X,'RHOAP =',E11.4,2X,'RHOBP =',E11.4,2X,'RHOCP =',E11	MAIN	20
6.4,6X,'G =',E11.4,/,3X,'VS =',E11.4,5X,'AK =',E11.4,5X,'HF =',E11.	MAIN	21
74,')	MAIN	22
40 FORMAT(5X,'P =',E11.4,5X,'C1 =',E11.4,3X,'BETA =',E11.4)	MAIN	23
50 FORMAT(1H,' CAPL =',E11.4,5X,'PA =',E11.4,5X,'PB =',E11.4,5X,'PC	MAIN	24
1 =',E11.4,5X,'V1 =',E11.4,3X,'RHOP =',E11.4,/,', RHO1 =',E11.4,2X,'	MAIN	25
2RHOJ1 =',E11.4,3X,'PRES =',E11.4)	MAIN	26
60 FORMAT(5X,'F =',E11.4,5X,'Y1 =',E11.4,2X,'DELY1 =',E11.4,5X,'P2 ='	MAIN	27
1,E11.4,' DELL1P =',E11.4)	MAIN	28
62 FORMAT(' RHO2 =',E11.4)	MAIN	29
70 FORMAT(3X,'PBP =',E11.4,5X,'BP =',E11.4,' DELLBP =',E11.4)	MAIN	30
80 FORMAT(4X,'Y2 =',E11.4,5X,'V2 =',E11.4,3X,'PRES =',E11.4,6X,'F =',	MAIN	31
1E11.4,2X,'DELY2 =',E11.4,5X,'P4 =',E11.4,/,', DELL2P =',E11.4,5X,'F	MAIN	32
2P =',E11.4)	MAIN	33
82 FORMAT(1H,'DELLA =',E11.4,' DELLB =',E11.4,' DELLC =',E11.4)	MAIN	34
90 FORMAT(4X,'PP =',E11.4,2X,'DELL1 =',E11.4,' DELL1P =',E11.4,2X,'DE	MAIN	35
1LL2 =',E11.4,' DELL2P =',E11.4,3X,'PPIN =',E11.4)	MAIN	36
92 FORMAT(1H,'DELL1 =',E11.4)	MAIN	37
94 FORMAT(3X,'PCP =',E11.4,5X,'CP =',E11.4,' DELLCP =',E11.4)	MAIN	38
96 FORMAT(3X,'PAP =',E11.4,5X,'AP =',E11.4,' DELLAP =',E11.4,2X,'DELL	MAIN	39
12 =',E11.4)	MAIN	40
98 FORMAT(' RHOPP =',E11.4,2X,'RHOJ2 =',E11.4,5X,'V2 =',E11.4)	MAIN	41
C *** CALCULATIONS	MAIN	42
C	MAIN	43
CVH2D = 2.007E7 \$ CV = 8.78E6 \$ VDET = 7.0E5	MAIN	44
WRITE(6,10)	MAIN	45
BX = 1.0 \$ BY = 1.0	MAIN	46
LAB(1) = 10H TONIHMA \$ LAB(2) = 10H X5742-309	MAIN	47
LAB(3) = 10H PLOT \$ LAB(4) = 10H SCOOP	MAIN	48
XPAGE = 8.0 \$ YPAGE = 8.0	MAIN	49
CALL PLTBEG(XPAGE,YPAGE,1.0,9,LAB)	MAIN	50
CALL PLOT(BX,BY,-3)	MAIN	51
BX = 0.0 \$ BY = 0.0	MAIN	52
CALL FACTOR(0.3)	MAIN	53
DO 3000 IC = 1,2	MAIN	54
DO 3000 IC = 2,2	MAIN	55
READ(5,20) A, B, BP, AP, CP, RADIUS, HP, AL, RHOZ, E, VT, VB,	MAIN	56
1 ALPHA, RHOT, VS, AK, HF	MAIN	57
A = 0.0 \$ B = 0.0 \$ AP = 0.0 \$ BP = 0.0 \$ CP = 0.0 \$ HP = 0.0	MAIN	58
RADIUS = 1.0 \$ AL = 0.20 \$ E = 0.40	MAIN	59
READ(5,25) ICOUNT	MAIN	60
READ(5,4) TITLE	MAIN	61
DO 700 LL = 1,ICOUNT	MAIN	62
	MAIN	63
	MAIN	64

WRITE(6,5) TITLE, LL	MAIN	65
WRITE(6,15)	MAIN	66
READ(5,20) C, D, H, RHOA, RHOB, RHOC, RHOAP, RHOBP, RHUCP, G	MAIN	67
READ(5,20) (GG(I), I=1,2)	MAIN	69
READ(5,20) (RRHO(I), I=1,9)	MAIN	70
DO 680 IG = 1,2	MAIN	71
G = GG(IG)	MAIN	72
DO 670 ID = 1,4	MAIN	73
CALL AXIS(0.0,0.0,4HC+CP,-4,10.0,0.0,0.0,0.2)	CORRB	1
CALL AXIS(0.0,0.0,2HPP,2,10.0,90.0,0.0,0.2)	MAIN	75
GAP = FLOAT(ID)	MAIN	76
DO 660 IRHO = 1,9	MAIN	78
RHOC = RRHO(IRHO)	MAIN	79
RHOCF = RHOC	CORRB	2
TPCC = 0	MAIN	80
DO 655 ICC = 1,41	MAIN	81
C = (ICC-1) * 2.0 / 40.0	MAIN	82
IF(C.EQ. 0.0) C = 0.001	MAIN	83
IF(C.GT. GAP) GO TO 655	MAIN	84
C = C / 2.0 \$ CP = C	CORRB	3
D = GAP - C - CP	CORRB	4
H = 0.0 \$ HP = 0.0	CORRB	5
RHOA = 0.0 \$ RHOAP = 0.0 \$ RHOB = 0.0 \$ RHOBP = 0.0	MAIN	86
IF(G.EQ. 0.209) HF = 5.762E9	MAIN	87
IF(G.EQ. 0.290) HF = 5.084E9	MAIN	88
IF(G.EQ. 1.0) HF = 3.333E9	MAIN	89
IF(G.EQ. 0.260) HF = 3.33E9	MAIN	90
IF(IC.EQ. 2) HP = H	MAIN	91
CAPL = RADIUS + H + A + B + C + D + AP + BP + CP + HP	MAIN	95
C1 = (VT-VB) / (AL*VB)	MAIN	96
P = 0.0	MAIN	97
DX = AL / 100.0	MAIN	98
X = DX / 2.0	MAIN	99
DO 100 I = 1,99	MAIN	100
IF(RHOZ.EQ. 0.0 .OR. RHOZ.EQ. 0.0) GO TO 150	MAIN	101
P = P + (SQRT(RHOZ/RHOA)) * DX * (1.0+(C1*CAPL+C1*P)/(1.0+C1*X))**	MAIN	102
10.5/(1.0+ALPHA*CAPL/E) ** 0.5	MAIN	103
X = X + DX	MAIN	104
100 CONTINUE	MAIN	105
C 150 WRITE(6,40) P, C1, BETA	MAIN	106
150 CONTINUE	MAIN	107
CAPL1 = H + A + C / 2.0	MAIN	108
PA = 0.0	MAIN	109
DX = AL / 100.0	MAIN	110
X = AL - DX / 2.0	MAIN	111
DO 200 I = 1,99	MAIN	112
IF(RHOZ.EQ. 0.0 .OR. RHOZ.EQ. 0.0) GO TO 210	MAIN	113
PA = PA + (SQRT(RHOZ/RHOA)) * DX * (1.0+(C1*H+C1*PA)/(1.0+C1*X))**0.5/	MAIN	114
1 (1.0+ALPHA*H/E) ** 0.5	MAIN	115
X = X - DX	MAIN	116
IF(PA.GE. A) GO TO 210	MAIN	117
200 CONTINUE	MAIN	118
210 DELLA = AL - X	MAIN	119
PC = 0.0	MAIN	120
BETA = 1.0	MAIN	121
CAPVS = 5.0E5	MAIN	122
DX = (AL-DELLA) / 100.0	MAIN	123
X = (AL-DELLA) - DX / 2.0	MAIN	124
DO 220 I = 1,99	MAIN	125
IF(RHOC.EQ. 0.0) GO TO 1050	MAIN	126
C	MAIN	127
C *** NEGATIVE BETA FOR DETONATION LAYER.	MAIN	128
C *** INCLUDES PRESSURE DROP WITH EXPANSION.	MAIN	129
C	MAIN	130

	IF(G.LT. 0.0) BETA = 1.0 - G * (C/(C+PC*VDET/CAPVS)) / (0.5*RHOC*	MAIN	131
	1RHOZ*VT*VT/((SQRT(RHOC)+SQRT(RHOZ))**2))	MAIN	132
	IF(BETA.LT. 0.0) BETA = 0.0	MAIN	133
	IF(G.LT. 0.0) GO TO 1050	MAIN	134
	RHOJ = RHOZ * E / ((E+ALPHA*(H+A+C))*(1.0+C1*(H+A+PC)/(1.0+C1*X)))	MAIN	135
	RO = RHOJ / RHOC	MAIN	136
	V8 = VB + (VT-VB) * X / AL	MAIN	137
	CAPVS = VJ / (1.0+SQRT(RHOC/RHOJ))	MAIN	138
	DGREEK = 2.0 * G * HF / CAPVS**2	MAIN	139
	AKK = 1.0	MAIN	140
	IF(G.GT. 0.0) AKK = 1.0 / (1.0+(1.0-G)*CV/(G*CVH20))	MAIN	141
C	IF(G.EQ. 1.0) GO TO 1000	MAIN	142
	TEMP = (0.5*RHOJ*RHOC*VJ*VJ/(2.0*(SQRT(RHOJ)+SQRT(RHOC))**2)) / ((MAIN	143
	11.0-G)*CV)	MAIN	144
	IF(TEMP.LT. 373.0) GO TO 1000	MAIN	145
	GO TO 1010	MAIN	146
1000	TEMP = 373.0	MAIN	147
1010	WORKEF = (TEMP-373.0) / TEMP	MAIN	148
	GAM = WORKEF * AKK	MAIN	149
	TFAC = 1.0 - (GAM/RO) * (1.0-GAM/RO) * (1.0-DGREEK)	MAIN	150
	IF(TFAC.LE. 0.0) GO TO 1030	MAIN	151
	GO TO 1040	MAIN	152
1030	BETA = 1.0	MAIN	153
	GO TO 1050	MAIN	154
1040	V = (1.0-SQRT(TFAC)) / (1.0-GAM/RO)	MAIN	155
	FRHO = SQRT(RO)	MAIN	156
	FRHO = (FRHO*FRHO+FRHO-1.0) / (1.0+FRHO)	MAIN	157
	BETA = 1.0 / (1.0+GAM*(V+V*FRHO-DGREEK))	MAIN	158
	IF(BETA.LT. 0.0) BETA = 0.0	MAIN	159
1050	RHO1 = BETA * RHOC	MAIN	160
	IF(RHO1.LT. RHOC) RHO1 = RHOC	MAIN	161
	IF(RHOZ.EQ. 0.0 .OR. RHO1.EQ. 0.0) GO TO 230	MAIN	162
	PC = PC + (SQRT(RHOZ/RHO1)) * DX * (1.0+(C1*(H+A+PC))/(1.0+C1*X))	MAIN	163
	1**0.5 / (1.0+ALPHA*(H+A)/E) ** 0.5	MAIN	164
	X = X - DX	MAIN	165
	IF(PC.GE. C) GO TO 230	MAIN	166
220	CONTINUE	MAIN	167
230	DELLC = AL - DELLA - X	MAIN	168
	PB = 0.0	MAIN	169
	DX = (AL-DELLA-DELLC) / 100.0	MAIN	170
	X = (AL-DELLA-DELLC) - DX / 2.0	MAIN	171
	DO 240 I = 1,99	MAIN	172
	IF(RHOZ.EQ. 0.0 .OR. RHO1.EQ. 0.0) GO TO 250	MAIN	173
	PB = PB + (SQRT(RHOZ/RHO1)) * DX * (1.0+(C1*(H+A+C+PB))/(1.0+C1*X))	MAIN	174
	1**0.5 / (1.0+ALPHA*(H+A+C)/E) ** 0.5	MAIN	175
	X = X - DX	MAIN	176
	IF(PB.GE. B) GO TO 250	MAIN	177
240	CONTINUE	MAIN	178
250	DELLB = AL - DELLA - DELLC - X	MAIN	179
	DELL1 = DELLA + DELLB + DELLC	MAIN	180
C	WRITE(6,92) DELL1	MAIN	181
C	WRITE(6,82) DELLA, DELLB, DELLC	MAIN	182
	RHOJ1 = RHOZ * E / ((1.0+C1*(H+A+B+C))/(1.0+C1*(AL-DELL1))) * (E+AL	MAIN	183
	1PHA*(AL-DELL1)))	MAIN	184
	E1 = E / (1.0+ALPHA*(H+A+B+C)/E)	MAIN	185
	QCOL = AK * E1 * RHOJ1	MAIN	186
	RCOL = RHO1 * B	MAIN	187
	DISS = B	MAIN	188
	DIS = B	MAIN	189
	RHOP = RHO1	MAIN	190
	IF(QCOL.LE. RCOL) GO TO 260	MAIN	191
	RCOL = RCOL + RHO1 * C	MAIN	192
	DISS = DISS + C	MAIN	193
	DIS = C	MAIN	194

RHOP = RHOC	MAIN	195
IF(QCOL .LE. RCOL) GO TO 260	MAIN	196
RCOL = RCOL + RHOA * A	MAIN	197
DISS = DISS + A	MAIN	198
DIS = A	MAIN	199
RHOP = RHOA	MAIN	200
IF(QCOL .LE. RCOL) GO TO 260	MAIN	201
IF(A+B+C .EQ. 0.0) GO TO 253	MAIN	202
RHOP = RCOL / (A+B+C)	MAIN	203
GO TO 255	MAIN	204
253 RHOP = 0.0	MAIN	205
255 GO TO 270	MAIN	206
260 IF(RCOL .EQ. 0.0) GO TO 265	MAIN	207
FF = (QCOL-RCOL) / RCOL	MAIN	208
GO TO 267	MAIN	209
265 FF = 0.0	MAIN	210
267 RCOL = RCOL - RHOP * DIS * FF	MAIN	211
DISS = DISS - DIS * FF	MAIN	212
IF(DISS .EQ. 0.0) GO TO 268	MAIN	213
RHOP = RCOL / DISS	MAIN	214
GO TO 270	MAIN	215
268 RHOP = 0.0	MAIN	216
270 CONTINUE	MAIN	217
V1 = VB + (VT-VB) * (1.0-DELL1/AL)	MAIN	218
PRES = 0.5 * RHOP * RHOJ1 * V1 * V1 / (SQRT(RHOP)+SQRT(RHOJ1))**2	MAIN	219
C WRITE(6,50) CAPL, PA, PB, PC, V1, RHOP, RHO1, RHOJ1, PRES	MAIN	220
F = 1.0 / (1.0+(SQRT(PRES/RHOJ1))/(ALPHA*V1))	MAIN	221
IF((A*RHOA+B*RHOB+C*RHO1) .EQ. 0.0) GO TO 274	MAIN	222
Y1 = AK * E1 * RHOJ1 / (1.0+E1/(A*RHOA+B*RHOB+C*RHO1))	MAIN	223
GO TO 276	MAIN	224
274 Y1 = 0.0	MAIN	225
276 DELY1 = -Y1 * (1.0-SQRT((1.0+ALPHA*D/E)/(1.0+ALPHA*F*D/E)))	MAIN	226
P2 = 0.0	MAIN	227
CAPL2 = H + A + B + C + D	MAIN	228
DX = (AL-DELL1) / 100.0	MAIN	229
X = (AL-DELL1) - DX / 2.0	MAIN	230
DO 300 I = 1,99	MAIN	231
P2 = P2 + DX * (1.0+C1*CAPL2/(1.0+C1*X))	MAIN	232
X = X - DX	MAIN	233
IF(P2 .GE. DELY1) GO TO 310	MAIN	234
300 CONTINUE	MAIN	235
310 DELL1P = AL - DELL1 - X	MAIN	236
C WRITE(6,60) F, Y1, DELY1, P2, DELL1P	MAIN	237
C WRITE(6,62) RHO2	MAIN	238
PBP = 0.0	MAIN	239
DX = (AL-DELL1-DELL1P) / 100.0	MAIN	240
X = (AL-DELL1-DELL1P) - DX / 2.0	MAIN	241
DO 400 I = 1,99	MAIN	242
IF(RHOZ .EQ. 0.0 .OR. RHOBP .EQ. 0.0) GO TO 410	MAIN	243
PBP = PBP + (SQRT(RHOZ/RHOBP)) * DX * (1.0+(C1*(CAPL2+PBP))/(1.0+C	MAIN	244
11*X)) ** 0.5 / (1.0+ALPHA*CAPL2/E) ** 0.5	MAIN	245
X = X - DX	MAIN	246
IF(PBP .GE. BP) GO TO 410	MAIN	247
400 CONTINUE	MAIN	248
410 DELLBP = AL - DELL1 - DELL1P - X	MAIN	249
C WRITE(6,70) PBP, BP, DELLBP	MAIN	250
PCP = 0.0	MAIN	251
BETA = 1.0	MAIN	252
DX = (AL-DELL1-DELL1P-DELLBP) / 100.0	MAIN	253
X = (AL-DELL1-DELL1P-DELLBP) - DX / 2.0	MAIN	254
DO 420 I = 1,99	MAIN	255
C	MAIN	256
C *** NEGATIVE BETA FOR DETONATION LAYER.	MAIN	257
C *** INCLUDES PRESSURE DROP WITH EXPANSION	MAIN	258

C	IF(RHOCP .EQ. 0.0) GO TO 2050	MAIN	259
	IF(G .LT. 0.0) BETA = 1.0 - G * (CP/(CP+PCP*VDET/CAPVS)) / (0.5*	MAIN	260
	1RHOCP*RHOZ*VT*VT/((SQRT(RHOCP)+SQRT(RHOZ))**2))	MAIN	261
	IF(BETA .LT. 0.0) BETA = 0.0	MAIN	262
	IF(G .LT. 0.0) GO TO 2050	MAIN	263
	RHOJ = RHOZ * E / ((E+ALPHA*(CAPL2+BP))*(1.0+C1*(CAPL2+BP+PCP)/(1.	MAIN	264
	10+C1*X)))	MAIN	265
	RO = RHOJ / RHOCP	MAIN	266
	VJ = VB + (VT-VB) * X / AL	MAIN	267
	CAPVS = VJ / (1.0+SQRT(RHOCP/RHOJ))	MAIN	268
	DGREEK = 2.0 * G * HF / CAPVS**2	MAIN	269
	AKK = 1.0	MAIN	270
	IF(G .GT. 0.0) AKK = 1.0 / (1.0+(1.0-G)*CV/(G*CVH20))	MAIN	271
C	IF(G .EQ. 1.0) GO TO 2000	MAIN	272
	TEMP = (0.5*RHOJ*RHOCP*VJ*VJ/(2.0*(SQRT(RHOJ)+SQRT(RHOCP))**2)) /	MAIN	273
	1 ((1.0-G)*CV)	MAIN	274
	IF(TEMP .LT. 373.0) GO TO 2000	MAIN	275
	GO TO 2010	MAIN	276
2000	TEMP = 373.0	MAIN	277
2010	WORKEF = (TEMP-373.0) / TEMP	MAIN	278
	GAM = WORKEF * AKK	MAIN	279
	TFAC = 1.0 - (GAM/RO) * (1.0-GAM/RO) * (1.0-DGREEK)	MAIN	280
	IF(TFAC .LE. 0.0) GO TO 2030	MAIN	281
	GO TO 2040	MAIN	282
2030	BETA = 1.0	MAIN	283
	GO TO 2050	MAIN	284
2040	V = (1.0-SQRT(TFAC)) / (1.0-GAM/RO)	MAIN	285
	FRHO = SQRT(RO)	MAIN	286
	FRHO = (FRHO*FRHO+FRHO-1.0) / (1.0+FRHO)	MAIN	287
	BETA = 1.0 / (1.0+GAM*(V*V*FRHO-DGREEK))	MAIN	288
	IF(BETA .LT. 0.0) BETA = 0.0	MAIN	289
2050	RHO2 = BETA * RHOCP	MAIN	290
	IF(RHO2 .LT. RHOCP) RHO2 = RHOCP	MAIN	291
	IF(RHOZ .EQ. 0.0 .OR. RHO2 .EQ. 0.0) GO TO 430	MAIN	292
	PCP = PCP + (SQRT(RHOZ/RHO2)) * DX * (1.0+C1*(CAPL2+BP+PCP) / (1.0	MAIN	293
	1+C1*X)) ** 0.5 / (1.0+ALPHA*(CAPL2+BP)/E) ** 0.5	MAIN	294
	X = X - DX	MAIN	295
	IF(PCP .GE. CP) GO TO 430	MAIN	296
420	CONTINUE	MAIN	297
430	DELLCP = AL - DELL1 - DELL1P - DELLBP - X	MAIN	298
C	WRITE(6,94) PCP, CP, DELLCP	MAIN	299
	PAP = 0.0	MAIN	300
	DX = (AL-DELL1-DELL1P-DELLBP-DELLCP) / 100.0	MAIN	301
	X = (AL-DELL1-DELL1P-DELLBP-DELLCP) - DX / 2.0	MAIN	302
	DO 440 I = 1,99	MAIN	303
	IF(RHOZ .EQ. 0.0 .OR. RHOAP .EQ. 0.0) GO TO 450	MAIN	304
	PAP = PAP + (SQRT(RHOZ/RHOAP)) * DX * (1.0+C1*(CAPL2+BP+CP+PAP)/(1	MAIN	305
	1.0+C1*X)) ** 0.5 / (1.0+ALPHA*(CAPL2+BP+CP)/E) ** 0.5	MAIN	306
	X = X - DX	MAIN	307
	IF(PAP .GE. AP) GO TO 450	MAIN	308
440	CONTINUE	MAIN	309
450	DELLAP = AL - DELL1 - DELL1P - DELLBP - DELLCP - X	MAIN	310
	DELL2 = DELLAP + DELLBP + DELLCP	MAIN	311
C	WRITE(6,96) PAP, AP, DELLAP, DELL2	MAIN	312
	V2 = VB + (VT-VB) * (AL-DELL1-DELL1P-DELL2) / AL	MAIN	313
	IF(AP+BP+CP .EQ. 0.0) GO TO 451	MAIN	314
	RHOFP = (AP*RHOAP+BP*RHOBP+CP*RHOCP) / (AP+BP+CP)	MAIN	315
	GO TO 452	MAIN	316
451	RHOFP = 0.0	MAIN	317
452	RHOJ2 = RHOZ * E / (((1.0+C1*(CAPL2+AP+BP+CP)/(1.0+C1*(AL-DELL1-	MAIN	318
	1DELL1P-DELL2))))*(E+ALPHA*(AL-DELL1-DELL1P-DELL2))))	MAIN	319
	E2 = E / (1.0+ALPHA*(CAPL2+AP+BP+CP)/E)	MAIN	320
	QCOL = AK * E2 * RHOJ2	MAIN	321
		MAIN	322

RCOL = RHOBP + AP	MAIN	323
DISS = AP	MAIN	324
DIS = AP	MAIN	325
RHOPP = RHOAP	MAIN	326
IF(QCOL .LE. RCOL) GO TO 460	MAIN	327
RCOL = RCOL + RHOCF * CP	MAIN	328
DISS = DISS + CP	MAIN	329
DIS = CP	MAIN	330
RHOPP = RHOCF	MAIN	331
IF(QCOL .LE. RCOL) GO TO 460	MAIN	332
RCOL = RCOL + RHOAP * AP	MAIN	333
DISS = DISS + AP	MAIN	334
DIS = AP	MAIN	335
RHOPP = RHOBP	MAIN	336
IF(QCOL .LE. RCOL) GO TO 460	MAIN	337
IF(AP+BP+CP .EQ. 0.0) GO TO 459	MAIN	338
RHOPP = RCOL / (AP+BP+CP)	MAIN	339
GO TO 455	MAIN	340
453 RHOP = 0.0	MAIN	341
455 GO TO 470	MAIN	342
460 IF(RCOL .EQ. 0.0) GO TO 465	MAIN	343
FF = (QCOL-RCOL) / RCOL	MAIN	344
GO TO 467	MAIN	345
465 FF = 0.0	MAIN	346
467 RCOL = RCOL - RHOPP * FF + DIS	MAIN	347
DISS = DISS - DIS * FF	MAIN	348
IF(DISS .EQ. 0.0) GO TO 468	MAIN	349
RHOPP = RCOL / DISS	MAIN	350
GO TO 470	MAIN	351
468 RHOP = 0.0	MAIN	352
470 CONTINUE	MAIN	353
PRES = 0.5*RHOPP*RHOJ2*V2*V2/(SQRT(RHOPP)+SQRT(RHOJ2))*2	MAIN	354
C WRITE(6,98) RHOPP, RHOJ2, V2	MAIN	355
FP = 1.0 / (1.0+(SQRT(PRES/RHOJ2))/(ALPHA*V2))	MAIN	356
IF((AP*RHOAP+BP*RHOBP+CP*RHOCF) .EQ. 0.0) GO TO 474	MAIN	357
Y2 = AK * E2 / (1.0+E2*RHOJ2/(AP*RHOAP+BP*RHOBP+CP*RHOCF))	MAIN	358
GO TO 476	MAIN	359
474 Y2 = 0.0	MAIN	360
476 DELY2 = -Y2 * (1.0-SQRT((1.0+ALPHA*HP/E)/(1.0+ALPHA*FP*HP/E)))	MAIN	361
P4 = 0.0	MAIN	362
DX = (AL-(DELL1+DELL1P+DELL2)) // 100.0	MAIN	363
X = 99.5 * DX	MAIN	364
DO 500 I = 1,99	MAIN	365
P4 = P4 + DX * (1.0+C1*CAPL/(1.0+C1*X))	MAIN	366
X = X - DX	MAIN	367
IF(P4 .GE. DELY2) GO TO 510	MAIN	368
500 CONTINUE	MAIN	369
510 DELL2P = AL - (DELL1+DELL1P+DELL2) - X	MAIN	370
C WRITE(6,80) Y2, V2, PRES, F, DELY2, P4, DELL2P, FP	MAIN	371
PP = 0.0	MAIN	372
DX = AL - (DELL1+DELL1P+DELL2+DELL2P)	MAIN	373
DX = DX / 100.0	MAIN	374
X = DX / 2.0	MAIN	375
DO 600 I = 1,99	MAIN	376
IF(RHOZ .EQ. 0.0 .OR. RHOT .EQ. 0.0) GO TO 650	MAIN	377
PP = PP + (SQRT(RHOZ/RHOT)) * DX * (1.0+(C1*CAPL+C1*PP)/(1.0+C1*X))	MAIN	378
1)**0.5/(1.0+ALPHA*CAPL/E) ** 0.5	MAIN	379
X = X + DX	MAIN	380
600 CONTINUE	MAIN	381
PPIN = PP / 2.54	MAIN	382
650 CONTINUE	CORRB	6
IF(C .GT. 2.0 .OR. PP .GT. 2.0) GO TO 655	MAIN	384
IPCC = IPCC + 1	MAIN	385
PLC(ICC) = C + CP \$ PLPP(ICC) = PP	CORRB	7

```

655 CONTINUE
    PLC(IPCC+1) = 0.0
    PLPP(IPCC+1) = 0.0
    PLC(IPCC+2) = 0.2
    PLPP(IPCC+2) = 0.2
    CALL LINE(PLC,PLP,IPCC,1,0,0)
660 CONTINUE
    CALL PLTPGE
670 CONTINUE
680 CONTINUE
700 CONTINUE
3000 CONTINUE
    STOP
    END

```

```

MAIN      388
MAIN      389
MAIN      390
MAIN      391
MAIN      392
MAIN      393
MAIN      394
MAIN      395
MAIN      396
MAIN      397
MAIN      398
MAIN      399
MAIN      400
MAIN      401

```


DISTRIBUTION LIST

<u>No. of Copies</u>	<u>Organization</u>	<u>No. of Copies</u>	<u>Organization</u>
12	Administrator Defense Technical Info Center ATTN: DTIC-DDA Cameron Station Alexandria, VA 22314	1	Commander US Army Aviation Research and Development Command ATTN: DRDAV-E 4300 Goodfellow Boulevard St. Louis, MO 63120
2	Chairman DOD Explosives Safety Board Room 856-C Hoffman Bldg 1 2461 Eisenhower Avenue ATTN: Dr. T. Zaker Mr. W. Queen Alexandria, VA 22331	1	Director US Army Air Mobility Research and Development Laboratory Ames Research Center Moffett Field, CA 94035
1	Commander US Army Materiel Development and Readiness Command ATTN: DRCDMD-ST 5001 Eisenhower Avenue Alexandria, VA 22333	1	Commander US Army Communications Rsch and Development Command ATTN: DRDCO-PPA-SA Fort Monmouth, NJ 07703
7	Commander US Army Armament Research and Development Command ATTN: DRDAR-TDC DRDAR-TSS DRDAR-LCE, Dr. R.F. Walker DRDAR-LCE, Dr. N. Slagg DRDAR-LCE, L. Avrami DRDAR-LCM, R. Rindner Dover, NJ 07801	1	Commander US Army Missile Command ATTN: DRDSMI-R Redstone Arsenal, AL 35898
2	Commander US Army Armament Materiel Readiness Command ATTN: DRSAR-LC, L. Ambrosini DRSAR-LEP-L Rock Island, IL 61299	1	Commander US Army Missile Command ATTN: DRSMI-YDL Redstone Arsenal, AL 35898
1	Director US Army ARRADCOM Benet Weapons Laboratory ATTN: DRDAR-LCB-TL Watervliet, NY 12189	1	Commander US Army Missile Command ATTN: DRSME-RK, Dr. R.G. Rhoades Redstone Arsenal, AL 35898
1	Commander US Army Electronics R & D Cmd Technical Support Activity ATTN: DELSD-L Fort Monmouth, NJ 07703	1	Commander US Army Tank Automotive Rsch and Development Command ATTN: DRDTA-UL Warren, MI 48090
		1	Director US Army TRADOC Systems Analysis Activity ATTN: ATAA-SL, Tech Lib White Sands Missile Range NM 88002

DISTRIBUTION LIST

<u>No. of Copies</u>	<u>Organization</u>	<u>No. of Copies</u>	<u>Organization</u>
1	Commander US Army Defense Ammunition Center and School ATTN: SARAC-DEV, J. Byrd Savanna, IL 61074	8	Commander Naval Surface Weapons Center ATTN: Mr. L. Roslund, R122 Mr. M. Stosz, R121 Code X211, Lib E. Zimet, R13 R.R. Bernecker, R13 J.W. Forbes, R13 S.J. Jacobs, R10 K. Kim, R13 Silver Spring, MD 20910
1	Commander US Army Research Office ATTN: Chemistry Division P.O. Box 12211 Research Triangle Park, NC 27709	4	Commander Naval Weapons Center ATTN: Dr. L. Smith, Code 3205 Dr. A. Amster, Code 385 Dr. R. Reed, Jr., Code 388 Dr. K. J. Graham, Code 3835 China Lake, CA 93555
1	Commander Office of Naval Research ATTN: Dr. J. Enig, Code 200B 800 N. Quincy Street Arlington, VA 22217	1	Commander Fleet Marine Force, Atlantic ATTN: G-4 (NSAP) Norfolk, VA 23511
1	Commander Naval Sea Systems Command ATTN: Mr. R. Beauregard, SEA 64E Washington, DC 20362	1	Commander AFRPL ATTN: Mr. R. Geisler, Code AFRPL MKPA Edwards AFB, CA 93523
1	Commander Naval Explosive Ordnance Disposal Facility ATTN: Technical Library Code 604 Indian Head, MD 20640	1	Commander Ballistic Missile Defense Advanced Technology Center ATTN: Dr. David C. Sayles P.O. Box 1500 Huntsville, AL 35804
1	Commander Naval Research Lab ATTN: Code 6100 Washington, DC 20375	1	Director Lawrence Livermore National Lab University of California ATTN: Dr. M. Finger Livermore, CA 94550
1	Commander Naval Surface Weapons Center ATTN: Code G13 Dahlgren, VA 22448		

DISTRIBUTION LIST

<u>No. of Copies</u>	<u>Organization</u>
1	Director Los Alamos National Lab ATTN: Dr. B. Craig, M Division P.O. Box 1663 Los Alamos, NM 87544
1	Schlumberger Well Services ATTN: Dr. C. Aseltine 5000 Gulf Freeway Houston, TX 77023

Aberdeen Proving Ground

Dir, USAMSAA
ATTN: DRXSY-D
DRXSY-MP, H. Cohen
Cdr, USATECOM
ATTN: DRSTE-TO-F
Dir, USACSL, Bldg 3516, EA
ATTN: DRDAR-CLB-PA

USER EVALUATION OF REPORT

Please take a few minutes to answer the questions below; tear out this sheet, fold as indicated, staple or tape closed, and place in the mail. Your comments will provide us with information for improving future reports.

1. BRL Report Number _____

2. Does this report satisfy a need? (Comment on purpose, related project, or other area of interest for which report will be used.)

3. How, specifically, is the report being used? (Information source, design data or procedure, management procedure, source of ideas, etc.) _____

4. Has the information in this report led to any quantitative savings as far as man-hours/contract dollars saved, operating costs avoided, efficiencies achieved, etc.? If so, please elaborate.

5. General Comments (Indicate what you think should be changed to make this report and future reports of this type more responsive to your needs, more usable, improve readability, etc.) _____

6. If you would like to be contacted by the personnel who prepared this report to raise specific questions or discuss the topic, please fill in the following information.

Name: _____

Telephone Number: _____

Organization Address: _____

